Path Invariant Controllers for a Quadrotor With a Cable-suspended Payload Using a Global Parameterization

Adeel Akhtar Sajid Saleem Jinjun Shan

***Abstract*—Payload delivery using unmanned aerial vehicles (UAVs) has attained central importance for smart logistics and transportation systems in the context of the fourth industrial revolution. This work considers the problem of designing a smooth dynamic feedback control law for a point mass payload suspended to a quadrotor and making the load to follow a large class of curves that includes both closed and non-closed curves. Typically, the load path following problem is solved using either a coordinate-free or a local-coordinate based approach. However, in this paper, we adopt an alternative methodology. First, we express the system dynamics in an extended Euclidean space using a global coordinate system. Secondly, we propose two families of functions that lead to the design of almost-global and local controllers in terms of region of convergence. We cast the load path following problem in the framework of set stabilization, and as a result, the proposed controllers make the given path an invariant manifold. The resulting controllers guarantee that once the suspended load converges to the path, it stays on the path indefinitely while satisfying other application-specific constraints. Finally, to complement the theoretical results, we provide a successful real-world experimental validation of the proposed controller on a Quanser QDrone UAV platform with a cable-suspended payload.**

I. Introduction

In recent years, multi-rotor unmanned aerial vehicles (UAVs), such as quadrotors, have gained increased popularity compared to fixed-wing UAVs because of their compact size, simple design, cost-effective structure, easy maneuverability, and vertical-takeoff-and-landing (VTOL) capabilities [1]–[3]. The quadrotors are the primary driver of innovation in traditional domains, namely, logistics, transportation, surveillance, and communication [4]. As an instance, quadrotors offer immense potential as drone base stations creating a dynamic radio access network for plugging coverage holes in terrestrial mobile and cellular networks [5]. Most use cases demand a payload-carrying ability from the quadrotors while maneuvering precisely along a preassigned path in potentially hazardous and cluttered environments, such as last-mile delivery, aerial photography, material transportation, emergency rescue mission [6], [7].

Primarily, two mechanisms exist for transporting a payload using a quadrotor, i.e., using a gripper mechanism or tethering [4], [8], [9]. The former approach uses an active attachment that provides extra degrees of freedom for load manipulation at the cost of increased inertia, while the latter approach is that of a passive attachment that offers agility and maneuverability of the platform but with a higher degree of under-actuation [10]. In this paper, we consider the control of the quadrotor system with a cable-suspended payload. The system as part of the experimental setup is shown in Figure 1. Designing a controller for this system is challenging due to its nonlinear and underactuated dynamics. A controller based on linearization or small-angle approximations suffers performance limitations as it enforces a restricted flight envelope [11]. The controller design technique proposed in this paper does not rely on small-angle assumptions.

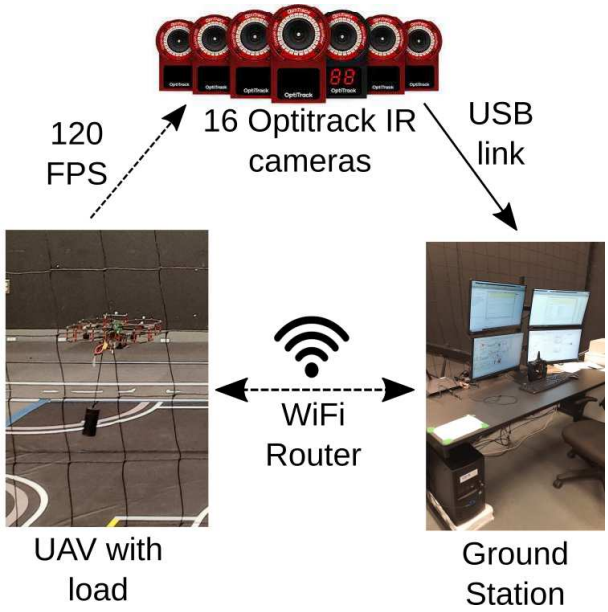

Fig. 1. The experimental setup consisting of 16 Optitrack cameras, a ground station, and QDrone UAV during flight with a cable-suspended payload.

In this paper, we consider a path following problem [12] of a point-mass suspended from a quadrotor. For a given non-self-intersecting smooth curve in the three-dimensional space, our objective is to propose a smooth dynamic controller such that the cable-suspended load converges to the given path and follows it. We assume that there exists a higher level path planning layer that generates such a path to be followed by the system [13], [14] . A path following problem and a trajectory tracking problem are related to each other, but the

This research was Supported by the Natural Sciences and Engineering Research Council of Canada (NSERC).

A. Akhtar and Jinjun Shan are with the Department of Earth and Space Science and Engineering, York University, 4700 Keele Street, Toronto, ON, Canada M3J 1P3 {a5akhtar;jjshan}@yorku.ca. Sajid Saleem is with the Georgia Institute of Technologies, Atlanta, GA ssaleem6@gatech.edu

former is more general since a path can be treated as a set of trajectories [15]. For example, there exist such instances where a path following problem can be solved, but the corresponding trajectory tracking problem has no solution [16], [17]. A key advantage of the path following framework is that it allows the system to achieve path invariance [18], i.e., once the system converges to the given path, it stays on the path indefinitely [19]. Moreover, path following approach precludes path planning and design of optimal trajectory characterized by the minimum jerk or minimum snap, which is a requirement for most of the trajectory tracking problems for the system under consideration [1]. Although path following approach has been applied to the quadrotor system [20], [21], there is no prior work that deals with the path following of the load suspended to a quadrotor through a cable for a class of curves.

The configuration space of the quadrotor and the tethered payload system is a product manifold, i.e., $\mathsf{SO}(3) \times \mathbb{S}^2 \times \mathbb{R}^m$, where $\mathsf{SO}(3)$ is a set of three-by-three orthogonal matrices called the special orthogonal group. Moreover, $\mathsf{SO}(3)$ is a three-dimensional smooth manifold with a Lie group structure. However, $\mathbb{S}^2$ is a two-dimensional manifold, and no Lie group structure can be defined on $\mathbb{S}^2$ [22]. The non-Euclidean nature and non-existing Lie group structure of the configuration space make the control design problem challenging. In literature, two approaches are primarily used to handle this situation, i.e., a geometric approach and a local-coordinate based approach [23]. A geometric approach, also called a coordinate-free approach, often leads to global solutions. However, it is impossible to design a global smooth feedback controller (see [24], [25]) on $\mathsf{SO}(3)$ because of topological obstructions [26]. In terms of the region of convergence, the best possible controllers are almost-global converging controllers [20], as their basin of attraction is the entire state space except a set of measure zero [23], [27]. It is well known that the smooth, compact manifold $\mathbb{S}^2$ also has an inevitable singularity, which makes it impossible to design a truly global smooth feedback controller on $\mathbb{S}^2$. Even the geometric approaches yield almost-global feedback laws valid on an open dense subset of $\mathbb{S}^2$ [28]. Since the configuration space of the quadrotor and the suspended payload system is a product manifold that involves both $\mathsf{SO}(3)$ and $\mathbb{S}^2$, therefore, it is impossible to design truly global smooth converging controllers for this system even with geometric approaches. Furthermore, for the system under study, all existing geometric control approaches adopt a hierarchical (cascade) approach that often assumes a time scale separation among each subsystem [10], [25]. Another shortcoming of almost every existing geometric control method for the given system is that they are intended to track a time-parameterized trajectory [10], [29]–[32], which has performance limitations as highlighted in [16]. Moreover, such trajectory tracking controllers cannot guarantee a precise path following in the sense that once the system converges to the trajectory, the system may leave the trajectory.

An alternative to the geometric framework is a local coordinate-based design method. Since an n-dimensional manifold is locally isomorphic to an n-dimensional Euclidean space, it can be locally represented using n parameters, also referred to as a local chart. It is impossible to find a three-dimensional chart for $\mathsf{SO}(3)$ that is both global and unique. In other words, every three-dimensional parameterization suffers singularities, such as gimbal lock [26], [33], [34]. Similarly, every two-dimensional parameterization of $\mathbb{S}^2$ also suffers singularities. In short, every local parameterization will lead to local controllers, i.e., the flight envelope of the quadrotor will be restricted such that the roll and the pitch angle are constrained to the interval $\left(-\frac{\pi}{2}, \frac{\pi}{2}\right)$.

In this paper, we propose a novel methodology that provides an alternative to both geometric and local-coordinate based approaches. First, we exploit the fact that each element of $\mathsf{SO}(3)$ is represented by a 3×3 rotational matrix, and treat each element of the rotation matrix as a parameter and express rotations of $\mathsf{SO}(3)$ as a nine-dimensional parameter vector in the extended space, which is both global and unique. Similarly, $\mathbb{S}^2$, which is embedded in $\mathbb{R}^3$, is expressed with three parameters in the extended space. Next, we express the system dynamics in the over parameterized space and formulate a path following problem in a unified setting. To the best of our knowledge, this is the first time a unified design approach is being proposed for the system under study. This design approach requires neither an assumption of time separation between quadrotor attitude dynamics and quadrotor position dynamics, nor a time-scale separation between the quadrotor and the load [20]. Moreover, another distinction between our work and the existing work is that we proposed a novel smooth dynamic feedback controller that guarantees path invariance. In other words, once the controller brings to the load to the path, the load stays on the path indefinitely, while maintaining the desired position, velocity, or acceleration profile. Given an *a priori* obstacle-free path, the proposed path following controller enables operation of quadrotor carrying the cable-suspended load in challenging environments that require aggressive maneuvers to avoid obstacles. Although the proposed approach can lead to a class of almost globally converging controllers, the over parameterization of the system causes uncontrolled internal dynamics. However, we show that these internal dynamics are well behaved and bounded.

Significantly less attention has been given to the path following problem compared to the trajectory tracking problem. In [35], the authors also consider a similar problem to the one we consider in this paper, i.e., a path following problem for a quadrotor system attached with a payload via suspended cable. A major distinction between our work and [35] is that the latter presents an inner-outer loop control approach based on reduction theorems, which allows the system to follow only straight lines. In [35], if the desired path is not straight, then it needs to be approximated by a series of straight lines, and the controller must switch from one segment to the other. Our proposed approach neither requires a piecewise approximation of the desired path nor switching while following challenging curves.

A. Contributions

We have made the following contributions.

1) The quadrotor and the cable-suspended load system model is represented using a novel parameterization that is both global and unique.

2) We propose two novel families $\mathscr{F}_R$ (Definition IV.5) and $\mathscr{F}_r$ (Definition IV.7) consisting of smooth functions that provide sufficient conditions to achieve well defined vector relative degree (Theorem V.1 and Theorem VI.1).
3) We propose novel dynamic transverse feedback linearizing controllers that allow the payload to achieve path invariance for a rich class consisting of both non-closed and closed curves.
4) Using a global and unique parameterization approach, we transform the system into a partial linear form with stable internal dynamics (Proposition V.5 and Proposition VI.3).
5) Validation of the proposed controller design through hardware implementation on an experimental platform consisting of a Quanser QDrone and a cable suspended load.

The rest of the paper is organized as follows. After presenting math preliminaries, we introduce the dynamic model of the quadrotor attached with cable-suspended load in Section II. The formal statement of the path following problem for the system under consideration is presented in Section III. In Section IV, we present a dynamic extension of the system and propose two novel families of path following maps. Section V and Section VI present theoretical results for vector relative degree of the system, its coordinate and feedback transformation using functions from the families $\mathscr{F}_R$ and $\mathscr{F}_r$, respectively. Numerical simulation results under practical scenarios are discussed in Section VII and conclusions are presented in Section IX.

B. Mathematical Notation

The symbol $:=$ denotes equal by definition. The set of natural number is denoted by $\mathbb{N}$. The standard n-dimensional Euclidean space is an $\mathbb{R}$-vector space denoted by $\mathbb{R}^n$ and it consists of ordered n-tuples $(x_1, \ldots, x_n)$, where each $x_i \in \mathbb{R}$, for $i \in \{1, 2, \ldots, n\}$. Sometimes it is convenient to represent elements of the Euclidean vector space as $n \times 1$ matrices, i.e., column vectors, and is denoted by $x = \mathrm{col}(x_1, \ldots, x_n)$, for $x \in \mathbb{R}^n$. Given $A \in \mathbb{R}^{m\times n}$, its transpose is denoted by $A^\top \in \mathbb{R}^{n\times m}$. The standard inner product on $\mathbb{R}^n$ is denoted by $\langle \cdot, \cdot \rangle : \mathbb{R}^n \times \mathbb{R}^n \to \mathbb{R}$, and the standard norm is denoted by $\| \cdot \| : \mathbb{R}^n \to \mathbb{R}$. A point to set distance, for a point $x \in \mathbb{R}$ and a set $S \subset \mathbb{R}^n$, is denoted by $\|x\|_S := \inf_{y\in S} \|x - y\|$. The cross product of two vectors in the three dimensional Euclidean space is denoted by $\times$. The composition of two functions, $\beta_1 : A_1 \to A_2$ and $\beta_2 : A_2 \to A_3$, is denoted by $\beta_2 \circ \beta_1 : A_1 \to A_3$. A parameterized curve σ in $\mathbb{R}^n$ is a map $\sigma : \mathbb{D} \to \mathbb{R}^n$, where the domain $\mathbb{D} = \mathbb{R}$ for non-closed curves, and $\mathbb{D} = \mathbb{R} \bmod P$ for closed curves of period P. For a P-periodic closed parameterized curve σ, $\sigma(\lambda + P) = \sigma(\lambda)$. Let $f : \mathbb{R}^n \to \mathbb{R}^m$ be a C^1 map and $p \in \mathbb{R}^n$, the derivative of f at p is denoted by $df_p := \frac{\partial f}{\partial x}\Big|_{x=p}$. For C^∞ maps $f, g : \mathbb{R}^n \to \mathbb{R}^n$ and a C^∞ map $\lambda : \mathbb{R}^n \to \mathbb{R}$, the iterative Lie derivatives are defined as $L_g^0\lambda := \lambda$, $L_g^k\lambda := L_g(L_g^{k-1}\lambda)$, $L_gL_f\lambda := L_g(L_f\lambda)$. The unit n-sphere is given by $\mathbb{S}^n = \left\{x \in \mathbb{R}^{n+1} : \|x\| = 1\right\}$. The set of all orientations of the rigid body is given by

$$\mathsf{SO}(3) = \left\{R \in \mathbb{R}^{3\times 3} : R^\top R = I, \det(R) = 1\right\},$$

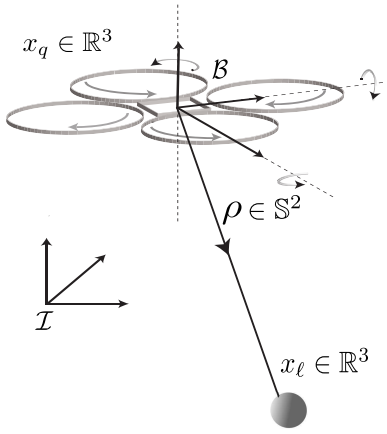

Fig. 2. Quadrotor schematic model with a cable-suspended payload

TABLE I
PARAMETERS, SYSTEM STATES AND NOTATION

Description	Symbols
Fixed inertial frame	$\mathcal{I} := \{e_1, e_2, e_3\}$
Quadrotor's body frame	$\mathcal{B} := \{b_1, b_2, b_3\}$
Constant cable length	$L \in \mathbb{R}$
Cable tension	$T \in \mathbb{R}$
Unit vector from quadrotor to the payload	$\rho \in \mathbb{S}^2$
Mass of the quadrotor and payload	$m_q \in \mathbb{R}$ and $m_\ell \in \mathbb{R}$
Position of the quadrotor and payload	$x_q \in \mathbb{R}^3$ and $x_\ell \in \mathbb{R}^3$
Velocity of the quadrotor and payload	$v_q \in \mathbb{R}^3$ and $v_\ell \in \mathbb{R}^3$
Thrust control input	$u_t \in \mathbb{R}$
Torque input of the quadrotor	$\tau := \mathrm{col}(\tau_1, \tau_2, \tau_3) \in \mathbb{R}^3$
Inertia of the quadrotor	$J := \mathrm{diag}(J_x, J_y, J_z) \in \mathbb{R}^{3\times 3}$
Acceleration due to gravity	$g \in \mathbb{R}$
Quadrotor body rates	$\Omega := \mathrm{col}(\Omega_1, \Omega_2, \Omega_3) \in \mathbb{R}^3$
Rotation matrix of the quadrotor	$R \in \mathsf{SO}(3)$
Parameterized curve	γ
Zero-level set representation of γ	$\mathcal{C}$
Path following manifold	$\mathcal{P}^\star$
Family of functions dependent on R	$\mathscr{F}_R$
Family of functions dependent on r	$\mathscr{F}_r$
Restricted vectorization operator on $\mathsf{SO}(3)$	$\Diamond\vert_{\mathsf{SO}(3)}$

The manifold $\mathsf{SO}(3)$ has an added Lie group structure and the corresponding Lie algebra is given by

$$\mathfrak{so}(3) = \left\{A \in \mathbb{R}^{3\times 3} : A = -A^\top\right\}.$$

The above set of skew-symmetric matrices has a vector space structure and is isomorphic to $\mathbb{R}^3$. The isomorphism is denoted by $\widehat{\cdot} : \mathbb{R}^3 \to \mathfrak{so}(3)$ and the inverse map is represented by $(\cdot)^\vee : \mathfrak{so}(3) \to \mathbb{R}^3$.

II. Dynamic Model

In this section, we describe the dynamical model of the system under consideration, i.e., the quadrotor with a cable-suspended point-mass, see Figure 2. First, we describe the model in a coordinate free form, and later we transform it using a global parameterization in the extended space.

The fixed inertial and body frame attached to the center of mass of the quadrotor are denoted by $\mathcal{I} := \{e_1, e_2, e_3\}$ and $\mathcal{B} := \{b_1, b_2, b_3\}$, respectively. The position and the velocity of the quadrotor are represented by $x_q(t) \in \mathbb{R}^3$ and $v_q(t) \in \mathbb{R}^3$,

respectively. Similarly, the position and velocity of the load are denoted by $x_\ell(t) \in \mathbb{R}^3$ and $v_\ell(t) \in \mathbb{R}^3$, while the mass of the load and the mass of the quadrotor are denoted by $m_\ell \in \mathbb{R}$ and $m_q \in \mathbb{R}$, respectively. Let the length of the cable be denoted by $L \in \mathbb{R}$, the tension in the cable be represented by $T \in \mathbb{R}$, and $g \in \mathbb{R}$ be the gravitational constant. We define the unit vector from the quadrotor to the load by $\rho(t) \in \mathbb{S}^2$, and this allows us to express the relationship between the position of the load and the position of the quadrotor as

$$x_q(t) = x_\ell(t) - L\rho(t). \tag{1}$$

The inertia and body rates of the quadrotor are represented by a diagonal matrix $J := \operatorname{diag}(J_x, J_y, J_z) \in \mathbb{R}^{3\times3}$ and the vector $\Omega(t) := \operatorname{col}(\Omega_1(t), \Omega_2(t), \Omega_3(t)) \in \mathbb{R}^3$, respectively.

Each propeller of the quadrotor produces a force, whose cumulative effect, also called the total thrust of the quadrotor, is represented by $u_t(t) \in \mathbb{R}$. The thrust force is assumed to be non-zero and along the b_3-axis, also referred to as z-axis. The quadrotor and the attached load is an underactuated system with four control inputs. The total moments about the three body-axes, defined by $\tau(t) := \operatorname{col}(\tau_1(t), \tau_2(t), \tau_3(t)) \in \mathbb{R}^3$, constitute the first three inputs of the quadrotor. The thrust $u_t(t)$ of the quadrotor is the fourth input of this system. The orientation is defined by a three-dimensional rotation matrix $R(t) \in \mathsf{SO}(3)$.

Assumption 1. We consider the following assumptions about the system:

1) The cable is inelastic and its mass is negligible relative to the mass of the load and the quadrotor, and
2) The cable tension is positive throughout the mission.

The equations of motion[1] of the quadrotor attached with the cable-suspended load is given as follows [36]:

$$\begin{aligned}
\dot{x}_\ell &= v_\ell \\
m_\ell \dot{v}_\ell &= -T\rho - m_\ell g b_3 \\
\dot{x}_q &= v_q \\
m_q \dot{v}_q &= u_t R b_3 - m_q g b_3 + T\rho \\
\dot{R} &= R\widehat{\Omega} \\
J\dot{\Omega} &= \tau - (\Omega \times J\Omega).
\end{aligned} \tag{2}$$

The configuration space of system (2) is $\mathsf{M} := \mathbb{R}^6 \times \mathsf{SO}(3)$, and the state space of system (2) is the tangent bundle $\mathsf{TM} \cong \mathbb{R}^{12} \times \mathsf{SO}(3) \times \mathbb{R}^3$ such that each element of TM is $(x_\ell, v_\ell, x_q, v_q, R, \Omega)$. It is well known that $\mathsf{SO}(3)$ is a three dimensional smooth manifold, hence locally represented by a three-dimensional chart, such as Euler angles. However, not all of $\mathsf{SO}(3)$ is covered by Euler angles, or for that matter, by any three dimensional parameterization [37]. A four-dimensional representation, such as quaternions, does not introduce any singularities, but they double cover the manifold $\mathsf{SO}(3)$. It has been shown that a five-dimensional representation expresses $\mathsf{SO}(3)$ as both globally and uniquely but results in a complicated set of coupled non-linear differential equations [38]. To overcome the issues mentioned above related to three-, four-, or five-dimensional parameterizations, we introduce a new parameterization for $\mathsf{SO}(3)$ [20]. This representation is both global and unique, which expresses each three-dimensional orthonormal matrix in $\mathsf{SO}(3)$ by a nine-dimensional coordinate. To this end, we introduce a vectorization operator $\lozenge$ that reshapes a three by three matrix A into a nine-dimensional column vector by the following transformation:

$$\begin{aligned}
\lozenge : \mathbb{R}^{3\times3} &\to \mathbb{R}^9 \\
A &\mapsto \operatorname{col}(Ae_1, Ae_2, Ae_3).
\end{aligned}$$

Note that $\lozenge$ is a linear and bijective map. However, when the domain is restricted to the manifold $\mathsf{SO}(3)$, the transformation fails to be an onto map. To resolve this issue, we define the restricted transformation such that the domain of the restricted operator is $\mathsf{SO}(3)$ and the co-domain is its image, i.e.,

$$\lozenge|_{\mathsf{SO}(3)} : \mathsf{SO}(3) \to \lozenge(\mathsf{SO}(3)).$$

Proposition II.1. *$\lozenge|_{\mathsf{SO}(3)} : \mathsf{SO}(3) \to \lozenge(\mathsf{SO}(3))$ is a global diffeomorphism.*

Proof. For proof, see [20]. □

For $R \in \mathsf{SO}(3)$, the $\lozenge|_{\mathsf{SO}(3)}$ when applied to R gives

$$\Xi := \lozenge|_{\mathsf{SO}(3)}(R) = \operatorname{col}(Re_1, Re_2, Re_3).$$

By substituting the value of ρ from (1) to (2) and after applying $\lozenge|_{\mathsf{SO}(3)}$ to (2), we can write

$$\begin{aligned}
\dot{x}_\ell &= v_\ell \\
\dot{v}_\ell &= -\frac{T}{m_\ell L}(x_\ell - x_q) - g b_3 \\
\dot{x}_q &= v_q \\
\dot{v}_q &= \frac{u_t}{m_q} R b_3 - g b_3 + \frac{T}{m_q L}(x_\ell - x_q) \\
\dot{\Xi} &= \lozenge|_{\mathsf{SO}(3)}(R\widehat{\Omega}) \\
\dot{\Omega} &= J^{-1}(\tau - (\Omega \times J\Omega)).
\end{aligned} \tag{3}$$

The state vector of the above system $x := \operatorname{col}(x_\ell, v_\ell, x_q, v_q, \Xi, \Omega)$ evolves on the manifold defined as $\bar{\mathsf{Q}} := \left\{\mathbb{R}^{12} \times (\operatorname{Im}(\lozenge|_{\mathsf{SO}(3)}) \subset \mathbb{R}^9) \times \mathbb{R}^3\right\} \subset \mathbb{R}^{24}$, which is a restricted Euclidean space. The inputs of the system are $\operatorname{col}(\tau_1, \tau_2, \tau_3, u_t) \in \mathbb{R}^4$ and are assumed to be continuously differentiable. We define the position of the point-mass (payload) in the inertial frame as the output of (3)

$$y = h(x) = x_\ell, \tag{4}$$

where $h : \mathbb{R}^{24} \to \mathbb{R}^3$ is a smooth map. A summary of system parameters and states is given in Table I.

III. Problem Formulation

Informally, in the path following problem of quadrotor attached with a cable-suspended load, the objective is to make the cable-suspended load converge to a given path and then follow it without leaving the path, using the four control inputs of the quadrotor. We call it the load path following problem. We highlight the fundamental difference between trajectory tracking and path following, i.e., a trajectory is

[1]Here, and throughout this paper, for simplicity of notation, we drop the time dependency of the state variables when describing the dynamics.

a time parameterized curve, while a path is considered as a set of points without any notion of time. We consider a parameterized curve γ, embedded in three-dimensional space

$$\begin{aligned}\gamma : \mathbb{D} &\to \mathbb{R}^3 \\ \lambda &\mapsto \operatorname{col}(\gamma_1(\lambda), \gamma_2(\lambda), \gamma_3(\lambda)).\end{aligned}$$

Furthermore, we assume that the given curve is regular, i.e., $\|\gamma'(\lambda)\| \neq 0$ for any $\lambda \in \mathbb{D}$. Any regular curve can be unit speed parameterized by its arc-length [19]. Therefore, without loss of generality, we assume γ to be a unit speed parameterized curve, i.e., $\|\gamma'(\lambda)\| = 1$. Similar to [37], we make the following assumption about the curve.

Assumption 2. Let $\mathcal{C} \subset \mathbb{R}^3$ be a one-dimensional embedded sub-manifold. Given any open set W, a C^∞ map $s : W \subset \mathbb{R}^3 \to \mathbb{R}^2$ exists such that $\mathcal{C} = s^{-1}(0)$ with $\operatorname{rank}(ds_y) = 2$, for all $y \in \mathcal{C}$.

As $\mathcal{C} = s^{-1}(0)$, for the system (3), the path in the output space (4) can be denoted by its zero-level set representation as

$$\mathcal{C} = s^{-1}(0) = \left\{ y \in \mathbb{R}^3 : s_1(y) = s_2(y) = 0 \right\}.$$

A. Problem statement

Given a quadrotor system attached with a cable-suspended load that satisfies Assumption 1 and a regular, embedded C^∞ curve $\mathcal{C}$ satisfying Assumption 2, design, if possible, a smooth dynamic feedback controller

$$\begin{aligned}\dot{z} &= \mathsf{A}(x, z) + \mathsf{B}(x, z)u \\ \begin{bmatrix}\tau \\ u_t\end{bmatrix} &= \mathsf{C}(x, z) + \mathsf{D}(x, z)u,\end{aligned} \tag{5}$$

with $z \in \mathbb{R}^k$, for some $k \in \mathbb{N}$ that needs to be determined, and $u \in \mathbb{R}^4$, such that if the quadrotor attached with the cable-suspended load is initialized in an open neighbourhood $\mathcal{U} \times \mathcal{V} \subset \mathbb{R}^{24} \times \mathbb{R}^k$ with $\mathcal{C} \subset h(\mathcal{U})$, the system achieves the following objectives:

- **P1** for each $(x(0), z(0)) \in \mathcal{U} \times \mathcal{V}$, the suspended payload converges to the desired path, i.e., $\|h(x(t))\|_{\mathcal{C}} \to 0$, as $t \to \infty$;
- **P2** the path $\mathcal{C} = s^{-1}(0)$ achieves output invariance, for all $t \geq 0$;
- **P3** on the path $\mathcal{C}$, the payload and quadrotor also satisfy miscellaneous requirements, i.e.,
  - point stabilization of the payload,
  - the speed, acceleration or jerk of the payload achieve a desired profile, and
  - the heading of the quadrotor satisfies a given reference profile;
- **P4** all internal states of the quadrotor with a cable-suspended load are bounded.

IV. Dynamic Extension and Path Following Maps

For a quadrotor attached with the cable-suspended load, our objective is to control the position of the payload, i.e., x_ℓ, and also heading of the quadrotor. It is shown in [25] that the payload position x_ℓ and heading of the quadrotor ψ constitute the flat outputs of the system under study. For the heading of the quadrotor, we need to put a constraint on the rotation matrix.

Next, we demonstrate that the quadrotor system with the cable-suspended load (3) fails to achieve a well-defined vector relative degree for any smooth function of x_ℓ and $\Diamond|_{\mathsf{SO}(3)}(R)$.

Proposition IV.1. *Given system (3) and the functions $\bar{\alpha}_i : \mathbb{R}^3 \to \mathbb{R}$, $x_\ell \mapsto \bar{\alpha}_i(x_\ell)$ for $i \in \{1, 2, 3\}$, and $\bar{\alpha}_4 : \mathbb{R}^3 \times \Diamond|_{\mathsf{SO}(3)} \subset \mathbb{R}^{12} \to \mathbb{R}$, $(x_\ell, \Diamond|_{\mathsf{SO}(3)}(R)) \mapsto \bar{\alpha}_4(x_\ell, \Diamond|_{\mathsf{SO}(3)}(R))$, the system fails to achieve a well-defined vector relative degree at any $x \in \bar{\mathsf{Q}} \subset \mathbb{R}^{24}$.*

Proof. See Appendix X-A. □

One way to interpret the rank deficient decoupling matrix in Proposition IV.1 is that the flow of the functions $\bar{\alpha}_i$ for $i \in \{1, \ldots, 4\}$ vanishes along the vector field $\bar{g}_1(x)$. This issue can be resolved by delaying the control input u_t using two integrators, which introduce two additional states $z = \operatorname{col}(z_1, z_2) \in \mathbb{R}_+ \times \mathbb{R}$. Let $u_t := z_1$, where z_1 is the first state of the dynamic controller. To delay the control input u_t one more time, we select $z_2 = u_d$, where u_d is the delayed control input. This leads to the following dynamic controller

$$\begin{aligned}\dot{z}_1 &= z_2 \\ \dot{z}_2 &= u_d.\end{aligned} \tag{6}$$

In other words, $\ddot{u}_t = u_d$. Let $u = \operatorname{col}(u_1, u_2, u_3, u_4) := \operatorname{col}(\tau_1, \tau_2, \tau_3, u_d)$. The augmentation of the two controller states to the system is called dynamic extension and the extended system is given by

$$\begin{aligned}\dot{x}_\ell &= v_\ell \\ \dot{v}_\ell &= -\frac{T}{m_\ell L}(x_\ell - x_q) - g b_3 \\ \dot{x}_q &= v_q \\ \dot{v}_q &= \frac{z_1}{m_q} R b_3 - g b_3 + \frac{T}{m_q L}(x_\ell - x_q) \\ \dot{\Xi} &= \Diamond|_{\mathsf{SO}(3)}(R\widehat{\Omega}) \\ \dot{\Omega} &= J^{-1}(\tau - (\Omega \times J\Omega)) \\ \dot{z}_1 &= z_2 \\ \dot{z}_2 &= u_d.\end{aligned} \tag{7}$$

For notational simplicity, we do not differentiate between the states of system (3) and the controller states (6), i.e., $(x_1, \ldots, x_{24})$ and (z_1, z_2). Let $x_{25} := z_1$, $x_{26} := z_2$ and $\mathsf{Q} := \bar{\mathsf{Q}} \times \mathbb{R}_+ \times \mathbb{R}$. Thus, the state vector for the extended system (7) is represented by $\mathbf{x} := \operatorname{col}(x_\ell, v_\ell, x_q, v_q, \Xi, \Omega, z_1, z_2) = \operatorname{col}(x_1, \ldots, x_{26}) \in \mathsf{Q} \subset \mathbb{R}^{26}$. For smooth vector fields

$$\begin{aligned}f(\mathbf{x}) := \operatorname{col}\Bigg(v_\ell, -\frac{T}{m_\ell L}(x_\ell - x_q) - g b_3, v_q, \frac{z_1}{m_q} R b_3 - g b_3 + \\ \frac{T}{m_q L}(x_\ell - x_q), \Diamond|_{\mathsf{SO}(3)}(R\widehat{\Omega}), J^{-1} - (\Omega \times J\Omega), 0, 0\Bigg),\end{aligned}$$

$g_1(\mathbf{x}) := \operatorname{col}\left(0_{21}, \frac{1}{J_x}, 0_4\right)$, $g_2(\mathbf{x}) := \operatorname{col}\left(0_{22}, \frac{1}{J_y}, 0_3\right)$, $g_3(\mathbf{x}) := \operatorname{col}\left(0_{23}, \frac{1}{J_z}, 0_2\right)$, and $g_4(\mathbf{x}) := \operatorname{col}(0_{25}, 1)$ in Q, the extended system (7) can be written as

$$\dot{\mathbf{x}} = f(\mathbf{x}) + \sum_{i=1}^{4} g_i(\mathbf{x}) u_i. \tag{8}$$

Next, we define

$$\begin{aligned} \mathbf{h} : \mathsf{Q} \subset \mathbb{R}^{26} &\to \mathbb{R}^3 \\ \mathbf{x} &\mapsto x_\ell, \end{aligned}$$

as the output of the extended system (8). To achieve the objectives **P1** and **P2**, we exploit the zero-level set representation of the given curve $\mathcal{C}$ and define

$$\begin{bmatrix} \alpha_1(\mathbf{x}) \\ \alpha_2(\mathbf{x}) \end{bmatrix} := s \circ \mathbf{h}(\mathbf{x}) = \begin{bmatrix} s_1 \circ \mathbf{h}(\mathbf{x}) \\ s_2 \circ \mathbf{h}(\mathbf{x}) \end{bmatrix}, \tag{9}$$

such that $\frac{\partial \alpha_i}{\partial x_j} = 0$, for $i \in \{1, 2\}$, and $j \in \{4, 5, \ldots, 26\}$. Loosely speaking, the maps α_1 and α_2 are solely dependent on x_ℓ.

The lift of the given path $\mathcal{C}$ to the state space of the quadrotor attached with the cable-suspended load system yields a submanifold of Q, i.e.,

$$\mathcal{P} := \{\mathbf{x} \in \mathsf{Q} : s_1(\mathbf{h}(\mathbf{x})) = s_2(\mathbf{h}(\mathbf{x})) = 0\}.$$

When all the states of the system, which include the quadrotor states and the states of the payload, converge to the set $\mathcal{P}$, the position of the payload x_ℓ converges to the path $\mathcal{C}$. However, there is no guarantee that the payload never leaves the path, once all the states of the system (7) converge to submanifold $\mathcal{P}$. In other words, the lifted path $\mathcal{P}$ is not an invariant set. Next, we define the path following manifold as an invariant set contained in $\mathcal{P}$ [39].

Definition IV.2. Given a path $\mathcal{C}$, the path-following manifold $\mathcal{P}^\star$ of (7) is the maximal controlled invariant submanifold contained in the lift of $\mathcal{C}$. Moreover, $\mathcal{P}^\star$ is a non-empty subset of $\mathcal{P}$, with dimension $n^\star \leq 26$. •

The path following manifold can be determined by the zero dynamics algorithm, i.e.,

$$\begin{aligned} \mathcal{P}^\star = \Big\{ \mathbf{x} \in \mathsf{Q} : &\alpha_1(\mathbf{x}) = \cdots = \alpha_1^{(6)}(\mathbf{x}) = \\ &\alpha_2(\mathbf{x}) = \cdots = \alpha_2^{(6)}(\mathbf{x}) = 0 \Big\}. \end{aligned} \tag{10}$$

The set $\mathcal{P}^\star$ can be interpreted as an ensemble of all maneuvers of the closed-loop system such that an input signal $u \in \mathbb{R}^4$ can be selected to restrict the evolution of the payload's position to the given path $\mathcal{C}$. Now, we state two elementary results, which will be subsequently used to prove the main result of this section.

Lemma IV.3 ([40]). *For three linearly independent vectors v_1,v_2, and v_3 all in $\mathbb{R}^3$, $\langle v_1, (v_2 \times v_3) \rangle \neq 0$.*

For $i \in \{1, 2\}$, let $d_{x_\ell} \alpha_i := \operatorname{col}\left(\frac{\partial \alpha_i}{\partial x_1}, \frac{\partial \alpha_i}{\partial x_2}, \frac{\partial \alpha_i}{\partial x_3}\right)$ and $\gamma' := \operatorname{col}\left(\frac{\partial \gamma_1}{\partial \lambda}, \frac{\partial \gamma_2}{\partial \lambda}, \frac{\partial \gamma_3}{\partial \lambda}\right)$.

Lemma IV.4 ([20]). *Given two smooth maps α_1 and α_2, as defined in (9), $\operatorname{span}\{d_{x_\ell}\alpha_1, d_{x_\ell}\alpha_2, \gamma'\} = \mathbb{R}^3$ for all $x_\ell \in \mathcal{C}$.*

To achieve **P3**, we invoke the parametric representation γ of the path $\mathcal{C}$ to define another function α_3 in the output space. Consider an open neighbourhood of the curve $\mathcal{C}$, denoted by $\mathcal{N}(\mathcal{C}) \subset \mathbb{R}^3$, such that the following condition is satisfied. Given an element y in the neighbourhood set $\mathcal{N}(\mathcal{C})$, there exists a unique $y^\star \in \mathcal{C}$ such that $\|y\|_{\mathcal{C}} = \|y - y^\star\|$. Given such an open set $\mathcal{N}(\mathcal{C})$, we can define the following map:

$$\begin{aligned} \varpi : \mathcal{N}(\mathcal{C}) &\to \mathbb{D} \\ y &\mapsto \arg \inf_{\lambda \in \mathbb{D}} \|y - \gamma(\lambda)\|. \end{aligned} \tag{11}$$

Using (11), the map α_3 is defined as

$$\alpha_3 := \varpi \circ \mathbf{h} : \mathbb{R}^{26} \to \mathbb{R}. \tag{12}$$

To specify a constraint on the heading of the quadrotor, first we define the following two mappings

$$\begin{aligned} \beta_1 : \mathsf{Q} &\to \Diamond(\mathsf{SO}(3)) \subset \mathbb{R}^9 \\ \mathbf{x} &\mapsto \beta_1(\mathbf{x}), \end{aligned} \tag{13}$$

and

$$\begin{aligned} \beta_2 : \Diamond(\mathsf{SO}(3)) &\to \mathbb{R} \\ \Diamond|_{\mathsf{SO}(3)}(R) &\mapsto \beta_2(Re_1, Re_2, Re_3). \end{aligned} \tag{14}$$

Definition IV.5. Given two smooth maps $\beta_1 : \mathsf{Q} \to \Diamond(\mathsf{SO}(3)) \subset \mathbb{R}^9$ and $\beta_2 : \Diamond(\mathsf{SO}(3)) \to \mathbb{R}$, and an open set $U_R \subset \mathsf{Q}$ containing $\mathbb{R}^{12} \times \Diamond(I_3) \times \mathbb{R}^3 \times \mathbb{R}_+ \times \mathbb{R}$, let $\alpha_4 := \beta_2 \circ \beta_1$ be such that on the set U_R, it satisfies the following property

$$\langle Re_1, d_{Re_2}\alpha_4 \rangle - \langle Re_2, d_{Re_1}\alpha_4 \rangle \neq 0.$$

All such α_4 constitute a family and we call it $\mathscr{F}_R$. •

Next, we consider an example function $\alpha_4 \in \mathscr{F}_R$.

Example IV.6. In this example we propose an α_4 function and characterize the domain on which it is defined. Let $\alpha_4 = r_{21} - r_{12}$. It is easy to check that $\langle Re_1, d_{Re_2}\alpha_4 \rangle - \langle Re_2, d_{Re_1}\alpha_4 \rangle = r_{11} + r_{22} \neq 0$ in a neighborhood of identity matrix I_3 and $\alpha_4 \in \mathscr{F}_R$ as long as the rotation matrix is from the set

$$U_\beta = \{R \in \mathsf{SO}(3) : \operatorname{trace}(R) > 1\}.$$

For details see [22, Proposition 5.7]. Using the above mentioned domain, the set U_R is defined as

$$U_R := \mathbb{R}^{12} \times \Diamond(U_\beta) \times \mathbb{R}^3 \times \mathbb{R}_+ \times \mathbb{R}.$$

△

Definition IV.7. Let $\alpha_4 : \mathsf{Q} \to \mathbb{R}$ be a smooth map. We call the map α_4 belong to the family $\mathscr{F}_r$ if it satisfies the following properties everywhere on Q

1) $\frac{\partial}{\partial r}\alpha_4 \neq 0$, and
2) $\frac{\partial}{\partial x_i}\alpha_4 = 0$, for $i \in \{1, \ldots, 26\} \setminus \{24\}$.

•

A simple example of $\alpha_4 \in \mathscr{F}_r$ is $\alpha_4(r) = r$. In the sequel, we will characterize vector relative degree and compute coordinate transformations using functions belonging to each $\mathscr{F}_R$ and $\mathscr{F}_r$ family.

V. Controller Design and $\mathscr{F}_R$ family

In this section, we consider the family $\mathscr{F}_R$, and our objective is to prove that the vector relative degree of system (8) is well defined and that its internal states are stable. To this end, first we select α_1 and α_2 satisfying Lemma IV.4, α_3 defined in (12) and for $\alpha_4 \in \mathscr{F}_R$, which together constitute a virtual output function $\mathbf{y}_R : U_R \subset \mathsf{Q} \to \mathbb{R}^4$ as

$$\mathbf{y}_R = \begin{bmatrix} \alpha_1 \\ \alpha_2 \\ \alpha_3 \\ \alpha_4 \end{bmatrix} = \begin{bmatrix} s_1 \circ \mathbf{h} \\ s_2 \circ \mathbf{h} \\ \varpi \circ \mathbf{h} \\ \beta_2 \circ \beta_1 \end{bmatrix}. \tag{15}$$

The following result establishes the vector relative degree of the quadrotor system attached with cable-suspended payload.

Theorem V.1. *The extended system (8) satisfying* Assumption 1*, with output defined in (15), achieves a well-defined vector relative degree everywhere on the set $\mathcal{P}^\star \cap U_R$, which is equal to $\{6, 6, 6, 2\}$.*

Proof. Let us consider $\mathbf{x}^\star \in \mathcal{P}^\star \cap U_R$ be an arbitrary element and let the path parameter $\lambda^\star \in \mathbb{D}$ be such that $h(\mathbf{x}^\star) = \gamma(\lambda^\star)$. By Definition IV.2, $\mathcal{P}^\star \subseteq \mathcal{P}$ and it implies that $h(\mathbf{x}^\star)$ is on the given path $\mathcal{C}$. By the definition of vector relative degree, we must establish that in a neighbourhood of $\mathbf{x}^\star$,

$$L_{g_i} L_f^j \alpha_k(\mathbf{x}) \equiv 0, L_{g_i} \alpha_4(\mathbf{x}) \equiv 0, \tag{16}$$

for $i \in \{1, 2, \ldots, 4\}$, $j \in \{0, \ldots, 4\}$, $k \in \{1, 2, 3\}$ and

$$D(\mathbf{x}) = \begin{bmatrix} L_{g_1} L_f^5 \alpha_1(\mathbf{x}) & \ldots & L_{g_4} L_f^5 \alpha_1(\mathbf{x}) \\ L_{g_1} L_f^5 \alpha_2(\mathbf{x}) & \ldots & L_{g_4} L_f^5 \alpha_2(\mathbf{x}) \\ L_{g_1} L_f^5 \alpha_3(\mathbf{x}) & \ldots & L_{g_4} L_f^5 \alpha_3(\mathbf{x}) \\ L_{g_1} L_f \alpha_4(\mathbf{x}) & \ldots & L_{g_4} L_f \alpha_4(\mathbf{x}) \end{bmatrix}, \tag{17}$$

is the full rank decoupling matrix. Through direct computation of Lie derivatives, we can establish that the condition (16) is satisfied. To show that the decoupling matrix is full rank, we analyze its determinant.

$$\begin{aligned} \det(D(\mathbf{x})) = &\left(\frac{T^3 z_1^2 \det(R)}{\det(J) L^3 m_\ell^3 m_q^3} \right) \\ &(r_{11} \partial_{r_{12}} \alpha_4 - r_{12} \partial_{r_{11}} \alpha_4 + \\ &r_{21} \partial_{r_{22}} \alpha_4 - r_{22} \partial_{r_{21}} \alpha_4 + \\ &r_{31} \partial_{r_{32}} \alpha_4 - r_{32} \partial_{r_{31}} \alpha_4) \\ &(\partial_{x_1} \alpha_1 (\partial_{x_2} \alpha_2 \gamma_3' - \partial_{x_3} \alpha_2 \gamma_2') + \\ &\partial_{x_2} \alpha_1 (\partial_{x_3} \alpha_2 \gamma_1' - \partial_{x_1} \alpha_2 \gamma_3') + \\ &\partial_{x_3} \alpha_1 (\partial_{x_1} \alpha_2 \gamma_2' - \partial_{x_2} \alpha_2 \gamma_1')), \end{aligned} \tag{18}$$

which can be further simplified as

$$\begin{aligned} \det(D(\mathbf{x})) = &\left(\frac{T^3 z_1^2}{\det(J) L^3 m_\ell^3 m_q^3} \right) \\ &(\langle Re_1, d_{Re_2} \alpha_4 \rangle - \langle Re_2, d_{Re_1} \alpha_4 \rangle) \\ &(\langle d_{x_\ell} \alpha_1, (d_{x_\ell} \alpha_2 \times \gamma') \rangle), \end{aligned} \tag{19}$$

since $\det(R) = 1$ for a rotation matrix R. The determinant of the decoupling matrix vanishes whenever any term in the numerator of (19) goes to zero or a factor in the denominator is infinity. The determinant of J, L, m_q and m_ℓ are positive finite constants. The tension in the string T is positive by Assumption 1. Since $\alpha_4 \in \mathscr{F}_R$, by Definition IV.5, $\langle Re_1, d_{Re_2} \alpha_4 \rangle - \langle Re_2, d_{Re_1} \alpha_4 \rangle \neq 0$. By Lemma IV.4, the $\text{span}\{d_{x_\ell} \alpha_1, d_{x_\ell} \alpha_2, \gamma'\} = \mathbb{R}^3$. Therefore, by Lemma IV.3, the $\langle d_{x_\ell} \alpha_1, (d_{x_\ell} \alpha_2 \times \gamma') \rangle \neq 0$. Also, $z_1 \neq 0$ everywhere on Q. Therefore, we have shown that the determinant of the decoupling matrix is non-zero for all $\mathbf{x}^\star \in \mathcal{P}^\star \cap U_R$ and the extended system (8) achieves a well defined vector relative degree of $\{6, 6, 6, 2\}$. □

Next, we define a coordinate transformation that partially linearizes the extended non-linear system. According to Theorem V.1, the cumulative vector relative degree of the system is 20, hence we require six additional functions to define a complete coordinate transformation.

Corollary V.2. *Let $\mathbf{x}^\star \in \mathcal{P}^\star \cap U_R$, then there exists an open set $U \subset \mathsf{Q}$ containing $\mathcal{P}^\star \cap U_R$ such that the mapping $\mathscr{T} : U \to \mathscr{T}(U)$, defined by*

$$\begin{bmatrix} \xi_i \\ \zeta_i \\ \eta_i \\ \mu_j \\ \delta_i \end{bmatrix} = \mathscr{T}(\mathbf{x}) = \begin{bmatrix} L_f^{i-1} \alpha_1(\mathbf{x}) \\ L_f^{i-1} \alpha_2(\mathbf{x}) \\ L_f^{i-1} \alpha_3(\mathbf{x}) \\ L_f^{j-1} \alpha_4(\mathbf{x}) \\ \delta_i(\mathbf{x}) \end{bmatrix}, \tag{20}$$

for $i \in \{1, \ldots, 6\}$ and $j \in \{1, 2\}$ is a diffeomorphism.

Proof. From the definition of virtual output functions (15) and their Lie derivatives, the expressions for ξ_i, ζ_i, η_i, and μ_j for $i \in \{1, \ldots, 6\}$ and $j \in \{1, 2\}$ can be determined. It should be noted that the distribution spanned by $\{g_1, \cdots, g_4\}$ is involutive. Thus, we select δ_i for $i \in \{1, \ldots, 6\}$ functions such that their derivatives annihilate this involutive distribution. We refer to these functions alternatively as δ-states or internal states. It is easy to see that the choice of δ-states is not unique, and here we present one particular choice, i.e.,

$$\begin{aligned} \text{col}(\delta_1, \delta_2, \delta_3) &:= Re_1 \\ \text{col}(\delta_4, \delta_5, \delta_6) &:= \text{col}(r_{22}, r_{32}, z_1). \end{aligned} \tag{21}$$

Given the internal states δ, as defined above, the next step towards establishing that $\mathscr{T}$ is diffeomorphism is to investigate the rank of the Jacobian matrix, i.e.,

$$\begin{aligned} \det\left(d_{\mathbf{x}} \mathscr{T}\right) = &\det(R) \left(\frac{T^{12} z_1^5}{L^{12} m_\ell^{12} m_q^6} \right) (\partial_{r_{12}} \alpha_4) \\ &(\langle Re_1, d_{Re_2} \alpha_4 \rangle - \langle Re_2, d_{Re_1} \alpha_4 \rangle) \\ &(\langle d_{x_\ell} \alpha_1, (d_{x_\ell} \alpha_2 \times \gamma') \rangle)^6. \end{aligned} \tag{22}$$

By definition of the family $\mathscr{F}_R$, $\langle Re_1, d_{Re_2} \alpha_4 \rangle - \langle Re_2, d_{Re_1} \alpha_4 \rangle \neq 0$ in an open set U_R. Similarly, by Theorem V.1, $\langle d_{x_\ell} \alpha_1, (d_{x_\ell} \alpha_2 \times \gamma') \rangle \neq 0$, and $z_1 \neq 0$ on Q. It should be noted that the Jacobian loses rank whenever $\partial_{r_{12}} \alpha_4$ is zero. However, this factor is dependent on the choice of the internal states which are non-unique. In other words, given a function $\alpha_4 \in \mathscr{F}_R$, we can make a careful choice of internal states such that $\partial_{r_{12}} \alpha_4 \neq 0$. Hence, $\mathscr{T}$ is a diffeomorphism everywhere on U. □

Remark V.3. For the function α_4 from Example IV.6, i.e., $\alpha_4 = r_{21} - r_{12}$, it is easy to see that the coordinate transformation $\mathscr{T}$ is a diffeomorphism everywhere on U_R.

Let the transformed states be represented by $\Psi := \text{col}(\xi, \zeta, \eta, \mu, \delta)$. Using Corollary V.2, the system (7) is locally differentially equivalent to four nonlinear subsystems with inputs and nonlinear uncontrolled internal dynamics given as follows:

$$\begin{aligned}
\dot{\xi}_1 &= \xi_2 \\
&\vdots \\
\dot{\xi}_5 &= \xi_6 \\
\dot{\xi}_6 &= L_f^6\alpha_1 + \sum_{k=1}^{4} L_{g_k}L_f^5\alpha_1 u_k\Big|_{\mathbf{x}=\mathscr{T}^{-1}(\Psi)},
\end{aligned} \tag{23}$$

$$\begin{aligned}
\dot{\zeta}_1 &= \zeta_2 \\
&\vdots \\
\dot{\zeta}_5 &= \zeta_6 \\
\dot{\zeta}_6 &= L_f^6\alpha_2 + \sum_{k=1}^{4} L_{g_k}L_f^5\alpha_2 u_k\Big|_{\mathbf{x}=\mathscr{T}^{-1}(\Psi)},
\end{aligned} \tag{24}$$

$$\begin{aligned}
\dot{\eta}_1 &= \eta_2 \\
&\vdots \\
\dot{\eta}_5 &= \eta_6 \\
\dot{\eta}_6 &= L_f^6\alpha_3 + \sum_{k=1}^{4} L_{g_k}L_f^5\alpha_3 u_k\Big|_{\mathbf{x}=\mathscr{T}^{-1}(\Psi)},
\end{aligned} \tag{25}$$

$$\begin{aligned}
\dot{\mu}_1 &= \mu_2 \\
\dot{\mu}_2 &= L_f^2\alpha_4 + \sum_{k=1}^{4} L_{g_k}L_f\alpha_4 u_k\Big|_{\mathbf{x}=\mathscr{T}^{-1}(\Psi)},
\end{aligned} \tag{26}$$

and

$$\dot{\delta}_i = b_i(\mathbf{x})|_{\mathbf{x}=\mathscr{T}^{-1}(\Psi)}, \tag{27}$$

where b_i are smooth maps for $i \in \{1, \ldots, 6\}$. The expressions (23), (24), (25), and (26) suggest the feedback

$$\begin{bmatrix} u_1 \\ u_2 \\ u_3 \\ u_4 \end{bmatrix} := D^{-1}(\mathbf{x}) \left(\begin{bmatrix} -L_f^6\alpha_1 \\ -L_f^6\alpha_2 \\ -L_f^6\alpha_3 \\ -L_f^2\alpha_4 \end{bmatrix} + \begin{bmatrix} v^\xi \\ v^\zeta \\ v^\eta \\ v^\mu \end{bmatrix} \right), \tag{28}$$

where $(v^\xi, v^\zeta, v^\eta, v^\mu)$ are auxiliary control inputs. The feedback transformation (28) reduces the extended nonlinear system to the following partial linear form

$$\begin{aligned}
&\dot{\xi}_1 = \xi_2 \quad \dot{\zeta}_1 = \zeta_2 \quad \dot{\eta}_1 = \eta_2 \quad \dot{\mu}_1 = \mu_2 \\
&\dot{\xi}_2 = \xi_3 \quad \dot{\zeta}_2 = \zeta_3 \quad \dot{\eta}_2 = \eta_3 \quad \dot{\mu}_2 = v^\mu \\
&\quad\vdots \qquad\quad \vdots \qquad\quad \vdots \qquad\quad \dot{\delta} = b(\Psi). \\
&\dot{\xi}_6 = v^\xi \quad \dot{\zeta}_6 = v^\zeta \quad \dot{\eta}_6 = v^\eta
\end{aligned} \tag{29}$$

The above system (29) consists of four decoupled linear subsystems, i.e., ξ-subsystem, ζ-subsystem, η-subsystem, and μ-subsystem, and an uncontrolled nonlinear dynamical subsystem, i.e., δ-subsystem, which we also refer as internal dynamics. Any linear controller design technique, such as the one presented in [20], [37], can be used to control the Ψ states, and therefore the objectives **P1**-**P3** are achieved. However, to satisfy **P4**, we need to establish that the internal states $\delta \in \mathbb{R}^6$ remain bounded.

A. Internal Dynamics

For the internal states defined in (21), we can calculate their dynamics, i.e.,

$$\begin{aligned}
\dot{\delta}_1(\Psi) &= rr_{12} - qr_{13}|_{\mathbf{x}=\mathscr{T}^{-1}(\Psi)} \\
\dot{\delta}_2(\Psi) &= rr_{22} - qr_{23}|_{\mathbf{x}=\mathscr{T}^{-1}(\Psi)} \\
\dot{\delta}_3(\Psi) &= rr_{32} - qr_{33}|_{\mathbf{x}=\mathscr{T}^{-1}(\Psi)} \\
\dot{\delta}_4(\Psi) &= pr_{23} - rr_{21}|_{\mathbf{x}=\mathscr{T}^{-1}(\Psi)} \\
\dot{\delta}_5(\Psi) &= pr_{33} - rr_{31}|_{\mathbf{x}=\mathscr{T}^{-1}(\Psi)} \\
\dot{\delta}_6(\Psi) &= z_2|_{\mathbf{x}=\mathscr{T}^{-1}(\Psi)}.
\end{aligned} \tag{30}$$

We present the following result to establish that the δ-states are bounded.

Lemma V.4. *The following system*

$$J\dot{\Omega} = \tau - (\Omega \times J\Omega),$$

is input-to-state stable.

Proof. For proof, see [41, Lemma VI.3]. □

The above Lemma leads to the following results.

Proposition V.5. *For the underactuated system (8) with bounded control inputs, $\tau \in \mathbb{R}^3$, the internal states δ_i and the internal dynamics $\dot{\delta}_i$, for $i \in \{1, \ldots, 6\}$, defined in (30) are bounded.*

Proof. See Appendix X-B. □

In summary, all four objectives, i.e., **P1**-**P4** are fulfilled, and the path following problem is solved. However, we underscore that the results of Theorem V.1 and Corollary V.2 are valid only on an open set U_R, which is dependent on the choice of $\alpha_4 \in \mathscr{F}_R$. Intuitively, the function α_4 controls the orientation of the quadrotor about the z-axis, or in terms of Euler angles, α_4 is related to the yaw angle of the quadrotor. The function presented in Example IV.6, i.e., $\alpha_4 = r_{21} - r_{12}$ poses a restriction that the orientation of the quadrotor about z-axis must be initialized in the open interval $(-\pi/2, \pi/2)$ and must remain in this open interval for all time. In other words, the quadrotor cannot perform one or more rotations about the z-axis, and the motion about z-axis is restricted to the open interval $(-\pi/2, \pi/2)$. However, this particular choice of α_4 does not restrict rotation about x and y axes, i.e., roll and pitch axes. To this end, it is an open problem to show whether there exist function(s) in the family $\mathscr{F}_R$ that allows the motion about z-axis on an interval $(-\pi, \pi)$? In other words, can we find a function α_4 belonging to the family $\mathscr{F}_R$ such that $U_R = \mathsf{Q} \backslash \mathsf{Z}$, where Z is a set of Lebesgue measure equal to zero?

To overcome this limitation of $\mathscr{F}_R$, we pick α_4 functions from the other family, i.e., $\mathscr{F}_r$. We will show in the next section that the given system still has a well-defined vector relative degree, and the quadrotor can even rotate about its z-axis in an unrestricted manner while satisfying all path following objectives.

VI. Controller Design and $\mathscr{F}_r$ family

In this section, we show that making an alternate choice of the virtual output function allows us to establish facts about the vector relative degree of the system (8) and its internal states, which are similar to those of the previous section when α_4 was selected from $\mathscr{F}_R$. However, this alternate choice, which consists of $\alpha_4 \in \mathscr{F}_r$, yields some virtual output functions that lead to a well-defined vector relative degree and coordinate transformation almost everywhere on the set Q.

Similar to Section V, first we select α_1 and α_2 satisfying Lemma IV.4, and α_3 as defined in (12). In contrast to Section V, we select $\alpha_4 \in \mathscr{F}_r$. Together these functions constitute a virtual output function $\mathbf{y}_r : U_r \subset \mathsf{Q} \to \mathbb{R}^4$ as

$$\mathbf{y}_r = \begin{bmatrix} \alpha_1 \\ \alpha_2 \\ \alpha_3 \\ \alpha_4 \end{bmatrix} = \begin{bmatrix} s_1 \circ \mathbf{h} \\ s_2 \circ \mathbf{h} \\ \varpi \circ \mathbf{h} \\ \alpha_4 \end{bmatrix}. \tag{31}$$

Theorem VI.1. *The extended system* (8) *satisfying* Assumption 1*, with output defined in* (31)*, achieves a well-defined vector relative degree of* $\{6,6,6,1\}$ *everywhere on the set* $\mathcal{P}^\star \cap U_r$.

Proof. Let us consider $\mathbf{x}^\star \in \mathcal{P}^\star \cap U_r$ be an arbitrary element and let the path parameter $\lambda^\star \in \mathbb{D}$ be such that $h(\mathbf{x}^\star) = \gamma(\lambda^\star)$. By Definition IV.2, $\mathcal{P}^\star \subseteq \mathcal{P}$ and it implies that the output $h(\mathbf{x}^\star)$ is on the given path $\mathcal{C}$. By the definition of vector relative degree, we must establish that in a neighbourhood of $\mathbf{x}^\star$,

$$L_{g_i} L_f^j \alpha_k(\mathbf{x}) \equiv 0,$$

for $i \in \{1,2,\dots,4\}$, $j \in \{0,\dots,4\}$, $k \in \{1,2,3\}$ and

$$\tilde{D}(\mathbf{x}) = \begin{bmatrix} L_{g_1} L_f^5 \alpha_1(\mathbf{x}) & \dots & L_{g_4} L_f^5 \alpha_1(\mathbf{x}) \\ L_{g_1} L_f^5 \alpha_2(\mathbf{x}) & \dots & L_{g_4} L_f^5 \alpha_2(\mathbf{x}) \\ L_{g_1} L_f^5 \alpha_3(\mathbf{x}) & \dots & L_{g_4} L_f^5 \alpha_3(\mathbf{x}) \\ L_{g_1} \alpha_4(\mathbf{x}) & \dots & L_{g_4} \alpha_4(\mathbf{x}) \end{bmatrix}, \tag{32}$$

is not rank deficient decoupling matrix. It is easy to see that

$$L_{g_i} L_f^j \alpha_k(\mathbf{x}) = 0$$

for $i \in \{1,2,3,4\}$, $j \in \{0,\dots,4\}$ and $k \in \{1,2,3\}$. To show that the decoupling matrix is full rank, we analyze its determinant.

$$\begin{aligned} \det(\tilde{D}(\mathbf{x})) = &\left(\frac{T^3 z_1^2}{\det(J) L^3 m_\ell^3 m_q^3} \right) (\partial_r \alpha_4) \\ &\left(\langle d_{x_\ell} \alpha_1, (d_{x_\ell} \alpha_2 \times \gamma') \rangle \right), \end{aligned} \tag{33}$$

Similar to the proof of Theorem V.1, the determinant of the decoupling matrix vanishes whenever any term in the numerator of (33) goes to zero or a factor in the denominator is infinity. Since $\alpha_4 \in \mathscr{F}_r$, by Definition IV.7, $\partial_r \alpha_4 \neq 0$ and using an argument similar to the proof of Theorem V.1, it can be shown that the determinant of the decoupling matrix is non-zero for all $\mathbf{x}^\star \in \mathcal{P}^\star \cap U_r$ and the extended system (8) achieves a well defined vector relative degree of $\{6,6,6,1\}$. □

Corollary VI.2. *Let* $\mathbf{x}^\star \in \mathcal{P}^\star \cap U_r$*, then there exists an open set* $U \subset \mathsf{Q}$ *containing* $\mathcal{P}^\star \cap U_r$ *such that the mapping* $\mathscr{D} : U \to \mathscr{D}(U)$*, defined by*

$$\begin{bmatrix} \tilde{\xi}_i \\ \tilde{\zeta}_i \\ \tilde{\eta}_i \\ \tilde{\mu}_1 \\ \tilde{\delta}_j \end{bmatrix} = \mathscr{D}(\mathbf{x}) = \begin{bmatrix} L_f^{i-1} \alpha_1(\mathbf{x}) \\ L_f^{i-1} \alpha_2(\mathbf{x}) \\ L_f^{i-1} \alpha_3(\mathbf{x}) \\ \alpha_4(\mathbf{x}) \\ \tilde{\delta}_j(\mathbf{x}) \end{bmatrix}, \tag{34}$$

for $i \in \{1,\dots,6\}$ *and* $j \in \{1,2,\dots,7\}$ *is a diffeomorphism.*

Proof. Computing the iterated Lie derivatives of the virtual output function in (15) along the vector field f, we obtain the closed-form expressions of $\tilde{\xi}_i$, $\tilde{\zeta}_i$, $\tilde{\eta}_i$, and $\tilde{\mu}_1$ for $i \in \{1,\dots,6\}$, which determine $\mathscr{D}$.

By using the virtual output function (15) and its Lie derivatives, we can determine the closed form expressions for the coordinate transformation $\mathscr{D}$, i.e., $\tilde{\xi}_i$, $\tilde{\zeta}_i$, $\tilde{\eta}_i$, and $\tilde{\mu}_1$ for $i \in \{1,\dots,6\}$. Similar to the proof of Corollary V.2, we pick seven $\tilde{\delta}$-states such that the involutive distribution spanned by $\operatorname{span}\{g_1,\dots,g_4\}$ is annihilated, i.e.,

$$\begin{aligned} \operatorname{col}(\tilde{\delta}_1, \tilde{\delta}_2, \tilde{\delta}_3) &:= Re_1 \\ \operatorname{col}(\tilde{\delta}_4, \tilde{\delta}_5, \tilde{\delta}_6) &:= Re_2 \\ \tilde{\delta}_7 &:= z_1. \end{aligned} \tag{35}$$

With the above choice of $\tilde{\delta}$ states, we check the rank of $d_{\mathbf{x}} \mathscr{D} \in \mathbb{R}^{26 \times 26}$, i.e.,

$$\begin{aligned} \det(d_{\mathbf{x}} \mathscr{D}) = \det(R) &\left(\frac{T^{12} z_1^5}{L^{12} m_\ell^{12} m_q^6} \right) (\partial_r \alpha_4) \\ &\left(\langle d_{x_\ell} \alpha_1, (d_{x_\ell} \alpha_2 \times \gamma') \rangle \right)^6. \end{aligned} \tag{36}$$

By definition of the family $\mathscr{F}_r$, $\partial_r \alpha_4 \neq 0$ in an open set U_r. Similarly, by Theorem V.1, $\langle d_{x_\ell} \alpha_1, (d_{x_\ell} \alpha_2 \times \gamma') \rangle \neq 0$, and $z_1 \neq 0$ on Q. Therefore, $\mathscr{D}$ is a diffeomorphism on U. □

Let $\tilde{\Psi} := \operatorname{col}(\tilde{\xi}, \tilde{\zeta}, \tilde{\eta}, \tilde{\mu}, \tilde{\delta})$ denote the transformed states. Theorem VI.1 allows us to pick a feedback

$$\begin{bmatrix} u_1 \\ u_2 \\ u_3 \\ u_4 \end{bmatrix} := \tilde{D}^{-1}(\mathbf{x}) \left(\begin{bmatrix} -L_f^6 \alpha_1 \\ -L_f^6 \alpha_2 \\ -L_f^6 \alpha_3 \\ -L_f \alpha_4 \end{bmatrix} + \begin{bmatrix} \tilde{v}^\xi \\ \tilde{v}^\zeta \\ \tilde{v}^\eta \\ \tilde{v}^\mu \end{bmatrix} \right), \tag{37}$$

where $(\tilde{v}^\xi, \tilde{v}^\zeta, \tilde{v}^\eta, \tilde{v}^\mu)$ are auxiliary control inputs and by Corollary VI.2, the extended nonlinear system takes the following partial linear form

$$\begin{aligned} \dot{\tilde{\xi}}_1 &= \tilde{\xi}_2 \quad \dot{\tilde{\zeta}}_1 = \tilde{\zeta}_2 \quad \dot{\tilde{\eta}}_1 = \tilde{\eta}_2 \quad \dot{\tilde{\mu}}_1 = \tilde{v}^\mu \\ \dot{\tilde{\xi}}_2 &= \tilde{\xi}_3 \quad \dot{\tilde{\zeta}}_2 = \tilde{\zeta}_3 \quad \dot{\tilde{\eta}}_2 = \tilde{\eta}_3 \quad \dot{\tilde{\delta}} = \tilde{b}(\tilde{\Psi}), \\ &\vdots \qquad\quad \vdots \qquad\quad \vdots \\ \dot{\tilde{\xi}}_6 &= \tilde{v}^\xi \quad \dot{\tilde{\zeta}}_6 = \tilde{v}^\zeta \quad \dot{\tilde{\eta}}_6 = \tilde{v}^\eta \end{aligned} \tag{38}$$

where $\tilde{b}$ are smooth functions. Since the above system consists of four chains of linear systems, we propose the following linear controllers.

$$\tilde{v}^{\xi} = \sum_{i=1}^{6} k_i^{\xi} \tilde{\xi}_i, \tag{39}$$

$$\tilde{v}^{\zeta} = \sum_{i=1}^{6} k_i^{\zeta} \tilde{\zeta}_i. \tag{40}$$

Controllers (39) and (40) make the path following manifold $\mathcal{P}^{\star}$ invariant and attractive, i.e., **P1** and **P2** are achieved by an appropriate choice of gains $k_i^{\xi}\tilde{\xi}_i$ and $k_i^{\zeta}\tilde{\zeta}_i$. To control the motion along the path, we propose the following controller

$$\tilde{v}^{\eta} = \sum_{i=1}^{6} k_i^{\eta}(\tilde{\eta}_i - \tilde{\eta}_i^{ref}). \tag{41}$$

By appropriate choice of k_i^{η} and η_i^{ref} using linear design tools, we can control the position, velocity, and acceleration of the payload along the curve. Finally, the body rate about the z-axis of the quadrotor is controlled by applying a similar technique on the $\tilde{\mu}$-system

$$\tilde{v}^{\mu} = k_1^{\mu}(\tilde{\mu}_1 - \tilde{\mu}_1^{ref}). \tag{42}$$

The controllers in (41) and (42) together achieve **P3**. To satisfy the final objective **P4**, we investigate the stability of the internal dynamics of the partial linear form (38).

A. Internal Dynamics

Similar to the previous section, we can determine the expressions for the internal dynamics from the internal states (21), i.e.,

$$\begin{aligned}
\dot{\tilde{\delta}}_1(\tilde{\Psi}) &= rr_{12} - qr_{13}|_{\mathbf{x}=\mathscr{D}^{-1}(\tilde{\Psi})} \\
\dot{\tilde{\delta}}_2(\tilde{\Psi}) &= rr_{22} - qr_{23}|_{\mathbf{x}=\mathscr{D}^{-1}(\tilde{\Psi})} \\
\dot{\tilde{\delta}}_3(\tilde{\Psi}) &= rr_{32} - qr_{33}|_{\mathbf{x}=\mathscr{D}^{-1}(\tilde{\Psi})} \\
\dot{\tilde{\delta}}_4(\tilde{\Psi}) &= pr_{13} - rr_{11}|_{\mathbf{x}=\mathscr{D}^{-1}(\tilde{\Psi})} \\
\dot{\tilde{\delta}}_5(\tilde{\Psi}) &= pr_{23} - rr_{21}|_{\mathbf{x}=\mathscr{D}^{-1}(\tilde{\Psi})} \\
\dot{\tilde{\delta}}_6(\tilde{\Psi}) &= pr_{33} - rr_{31}|_{\mathbf{x}=\mathscr{D}^{-1}(\tilde{\Psi})} \\
\dot{\tilde{\delta}}_7(\tilde{\Psi}) &= z_2|_{\mathbf{x}=\mathscr{D}^{-1}(\tilde{\Psi})}.
\end{aligned} \tag{43}$$

The following result establishes the internal states are bounded.

Proposition VI.3. *If the underactuated system (8) has bounded inputs, then the internal states and the internal dynamics in (43) remain bounded.*

Proof. Proof is similar to that of Proposition V.5 and hence omitted. □

In the light of the above Proposition VI.3, **P4** is also achieved, and hence the load path following problem is solved.

Example VI.4. Consider the virtual output function with a sinusoidal path in (x_1, x_2) plane at a height of 10 units along x_3-axis, and a reference body rate of r^{ref}, i.e.,

$$\mathbf{y}_r(\mathbf{x}) = \begin{bmatrix} \alpha_1(\mathbf{x}) \\ \alpha_2(\mathbf{x}) \\ \alpha_3(\mathbf{x}) \\ \alpha_4(\mathbf{x}) \end{bmatrix} = \begin{bmatrix} x_2 - \sin(x_1) \\ x_3 - 10 \\ x_1 \\ x_{24} - r^{ref} \end{bmatrix}. \tag{44}$$

We first investigate the conditions of Theorem VI.1. It can be seen that the

$$\det(\tilde{D}(\mathbf{x})) = \left(\frac{T^3 z_1^2}{J_1 J_2 J_3 L^3 m_\ell^3 m_q^3} \right) \neq 0, \tag{45}$$

for all $\mathbf{x}$ in Q. In other words, the open set $U_r = \mathsf{Q}$, is the entire state space. Next, we determine the neighborhood in which the coordinate transformation is well defined. We look at the conditions of Corollary VI.2

$$d_{\mathbf{x}}\mathscr{D} = \det(R) \left(\frac{T^{12} z_1^5}{L^{12} m_\ell^{12} m_q^6} \right) \neq 0, \tag{46}$$

for all $\mathbf{x}$ in Q. In summary, the choice of α_4 from the family $\mathscr{F}_r$ solves the load path following problem in the entire state space and removes the limitations of the $\mathscr{F}_R$ family. In other words, given appropriate α_1, α_2, and α_3, we can select an α_4 function from $\mathscr{F}_r$ that guarantees a coordinate and feedback transformation everywhere in the state space Q. △

It should be noted that by choosing a function α_4 belonging to $\mathscr{F}_r$ family, we can control the body rate of the quadrotor about the z-axis. However, a limitation of this selection is that we cannot set the quadrotor at a desired orientation along the z-axis. The $\mathscr{F}_R$ family does not suffer from this limitation, i.e., the orientation itself can be controlled rather than its rate, but the feedback and coordinate transformation are defined only on an open subset of state space in the neighborhood of the given path. Thus, the two proposed families of functions offer complementary choices for the design of the controller. Further investigation might yield functions in $\mathscr{F}_R$ that allows coordinate transformation in the entire (or almost-entire) state space.

VII. Simulation Results

In this section, we present simulation results of the quadrotor system attached with a cable-suspended payload for two scenarios. First, we present the case when the task is to follow a given closed path such that $\alpha_4 \in \mathscr{F}_R$. Next, we investigate the case when the system follows a non-closed curve such that $\alpha_4 \in \mathscr{F}_r$ in the presence of parametric uncertainties and sensor noise.

A. Path following of a closed curve

The goal is to make the suspended load follow the given parametric curve

$$\lambda \mapsto \mathrm{col}(4\cos(\lambda), 4\sin(\lambda), 10),$$

using $\alpha_4 \in \mathscr{F}_R$ presented in Example IV.6, i.e., $\alpha_4 = r_{21} - r_{12} = x_{16} - x_{14}$. In other words, the target is to make the

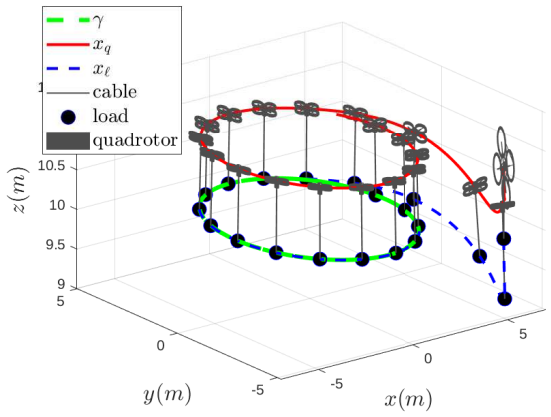

Fig. 3. Position of quadrotor and the cable-suspended load in the output space

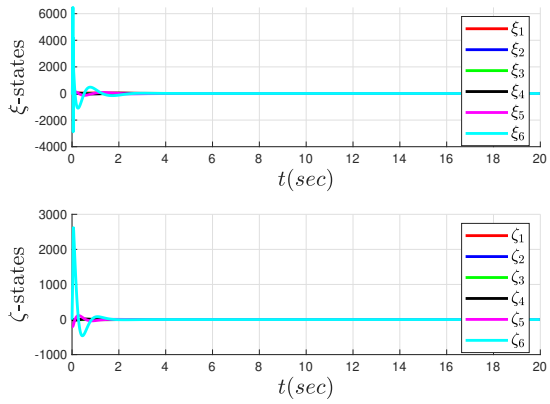

Fig. 4. Trajectories of ξ and ζ states

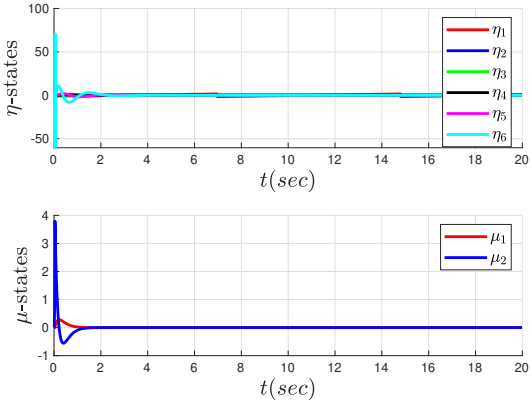

Fig. 5. Trajectories of η and μ states

cable-suspended load converge and follow the path specified by the virtual output function

$$\mathbf{y}_R(\mathbf{x}) = \begin{bmatrix} x_1^2 + x_2^2 - 16 \\ x_3 - 10 \\ \tan^{-1}(\frac{x_2}{x_1}) \\ x_{16} - x_{14} \end{bmatrix}. \tag{47}$$

The path following maneuver is shown in Figure 3. The desired path γ is shown by the dotted green line, and the path traversed by the load is shown by the solid blue line. The path traversed by the quadrotor for this mission is shown by a solid red line. Figure 3 shows the time snapshots of the quadrotor with the cable-suspended load at every second. The cable is represented by the grey line, and the load is represented by a solid black blob. As seen in the figure, the cable-suspended load is initialized away from the desired path, i.e., $x_\ell(0) = \text{col}(5, -5, 10)$, and the controllers (39) and (40) force the load to converge to the desired path. The initial velocity of the load and quadrotor is zero. The quadrotor is initialized at the following orientation

$$R(0) = \begin{bmatrix} 1 & 0 & 0 \\ 0 & 0.0175 & 0.9998 \\ 0 & -0.9998 & 0.0175 \end{bmatrix}, \tag{48}$$

which in terms of local coordinates, corresponds to an initial roll angle of -89° with pitch and yaw angles equal to zero. It should be noted that the initial conditions are defined in the set U_R. Although U_R is a slightly restricting set, it still allows the system to perform challenging maneuvers. This is a clear advantage of the family $\mathscr{F}_R$, in comparison to any other control scheme that uses small-angle assumption. Starting from this initial condition, not only, the load converges to the set $\mathcal{P}$, but it converges to $\mathcal{P}^\star$. Since $\mathcal{P}^\star$ is invariant, the load never leaves the set, i.e., the load stays on the path for all future time. Another way to interpret the stability of the set $\mathcal{P}^\star$ is to investigate the state trajectories of the ξ- and ζ-subsystem. As seen in Figure 4, all the ξ, and ζ states converge to zero, i.e., the suspended payload converges to the path, and it stays on the path indefinitely. The motion along the path is governed by the η-subsystem. The goal in this simulation is to follow the desired path with a constant angular velocity of 0.5 rad/sec in the counterclockwise direction, i.e., $\eta_2 - 0.5 = 0$. It can be seen in the top plot of Figure 5 that η_2 converges to the desired speed of 0.5 rad/sec. This makes η_1 evolve freely, while the states $\eta_3, \ldots, \eta_6$ approach zero, as illustrated in Figure 5. We want to highlight that the function α_4 is not just an arbitrary function but it has a physical meaning, i.e., when $\alpha_4 = r_{21} - r_{12} = 0$, the heading of the quadrotor goes to zero. As seen in the bottom plot of Figure 5, both μ_1 and μ_2, which correspond to α_4 and $\dot{\alpha}_4$, converge to zero. Finally, in Figure 6, it is shown that all the internal states, i.e., δ-states remain bounded.

B. Path following of a non-closed curve with noise

In this subsection, we consider the path following problem for the quadrotor tethered to a load in the context of a practical scenario. The imperfections in practical situation are modeled by the presence of noise in sensing the state and the uncertainties in the system parameters. We assume 1% of parametric uncertainties for m_q, m_ℓ, and L as these parameters can be precisely measured. However, we assume 10% parametric uncertainties for the inertia matrix of the quadrotor as it is difficult to accurately measure the inertia matrix.

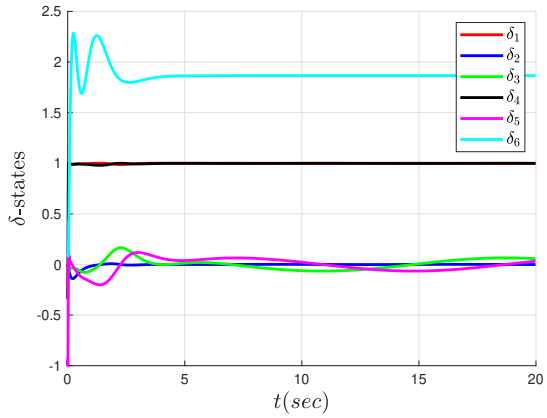

Fig. 6. Trajectories of the internal δ states

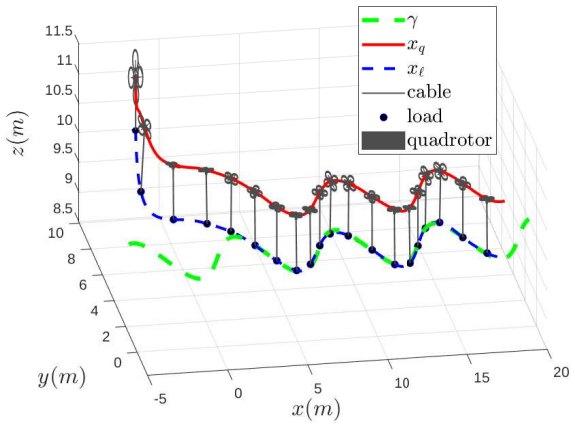

Fig. 7. Position of quadrotor and the cable-suspended load in the output space

We assume that the quadrotor is equipped with a standard inertial measurement unit (IMU) and an on-board computer that acquires measurements of angles of the quadrotor and the body rates. Moreover, we assume that the quadrotor is operating in an indoor arena equipped with a motion capture system that can measure position and velocity of the load and quadrotor. We simulate the system under practical noise levels for these sensors, for details see [42].

Considering the above mentioned parametric uncertainties and sensor noise, the task is to make the cable-suspended load follow the non-closed curve

$$\lambda \mapsto \mathrm{col}(\lambda, 1.5\sin(\lambda), 10).$$

For this scenario, we select $\alpha_4 = r - 0.5 = x_{24} - 0.5$, a function from the family $\mathscr{F}_r$, which is also the function considered in Example VI.4. In other words, the target is to make the cable-suspended load converge and follow the given path

$$\mathbf{y}_r(\mathbf{x}) = \begin{bmatrix} x_2 - 1.5\sin(x_1) \\ x_3 - 10 \\ x_1 \\ x_{24} - 0.5 \end{bmatrix}. \tag{49}$$

The system is initialized at a challenging initial position of $x_\ell(0) = \mathrm{col}(-1.5, 10, 10)$, and the pose of the quadrotor is initialized as defined by the rotation matrix

$$R(0) = \begin{bmatrix} 1 & 0 & 0 \\ 0 & -0.3420 & 0.9397 \\ 0 & -0.9397 & -0.3420 \end{bmatrix}, \tag{50}$$

which corresponds to an initial roll angle of -110° with pitch and yaw angles equal to zero. Figure 7 shows that the load converges to the path and then stays on the path. Figure 8 shows that both $\tilde{\xi}$- and $\tilde{\zeta}$- states converge to zero, i.e., the path following manifold $\mathcal{P}^\star$ achieves stability. Next, we present the state trajectory plots of the $\tilde{\eta}$- and $\tilde{\mu}$-subsystem. As seen in the top plot of the Figure 9, $\tilde{\eta}_2$ converges to the desired value, while $\tilde{\eta}_1$ is evolving freely. The rest of the $\tilde{\eta}$ states get close to zero. The convergence of $\tilde{\eta}_6$ is more sensitive to noise due to the sixth-order derivative of the position of the load. We want

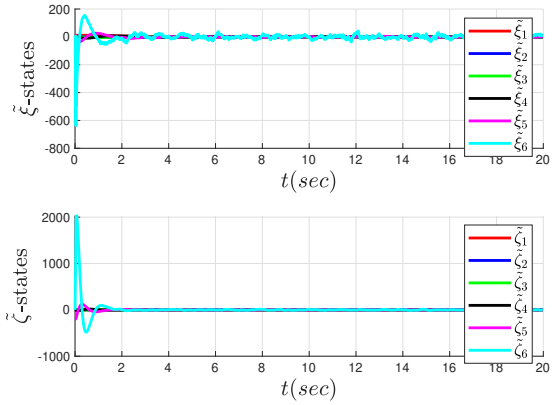

Fig. 8. Trajectories of $\tilde{\xi}$ and $\tilde{\zeta}$ states

to highlight that in the presence of given noise levels in $\tilde{\eta}_6$, the load precisely follows the path. Similarly, in the bottom plot of Figure 9, the state $\tilde{\mu}_1$ converges to zero, which implies that the quadrotor will spin about z-axis at the desired rate of 0.5 rad/sec. Finally, Figure 10 shows that the internal states remain bounded.

VIII. Experimental Results

In this section, we present practical results of successful hardware implementation of the proposed controller on a Quanser QDrone UAV[2] carrying a load attached to it with an inelastic cable. The Quanser QDrone is a mid-sized UAV supporting on-board compute resources, i.e., Intel® Aero Compute Board. Moreover, the UAV has an board 4GB LP-DDR3-1600 memory. UAV is protected by a carbon fiber frame, which is impact resistant. First we present the details of the experimental setup, and then follow it up with a discussion about the results of the experiment.

A. Experiment Design

The experiment is performed in an indoor laboratory environment that consists of a UAV QDrone with a cable

[2]https://www.quanser.com/products/qdrone/

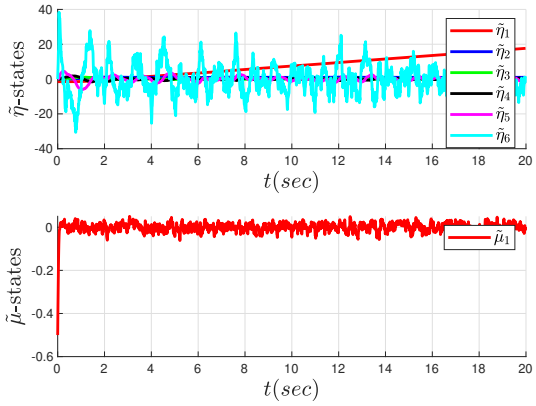

Fig. 9. Trajectories of the $\tilde{\eta}$ and $\tilde{\mu}$ states

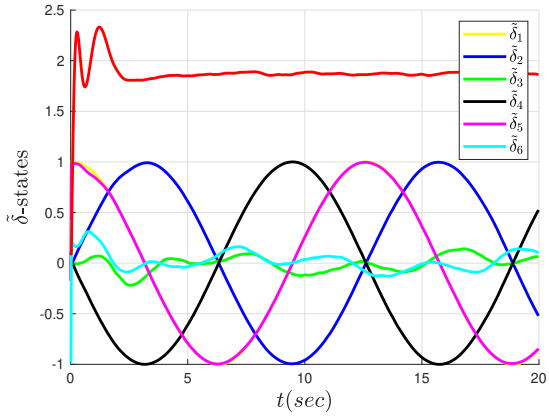

Fig. 10. Trajectories of $\tilde{\delta}$ states

suspended payload, a flight arena with dimensions 10m $\times$ 6m $\times$ 11m, and a camera systems consisting of 16 Natural Point Optitrack Flex-13 cameras, and a ground station as shown in Figure 1. The camera system provides precise low latency optical feedback at the rate of 100 Hz and covers the arena. The Natural Point Optitrack cameras feed information to the ground station that optimally computes the state of the dynamic system.

The dimensions of QDrone are 40 $\times$ 40 $\times$ 15 cm, and it weighs around 850g with batteries. The maximum payload capacity of QDrone is 300g. QDrones are equipped with four high-speed Electronic Speed Controlled (ESC) brushless motors with Hall-effect sensor outputs. The drone has a 3-axis 16-bit accelerometer, range configurable for $\pm$2g to $\pm$16g, a 3-axis gyroscope, range configurable for $\pm$125 deg/s to $\pm$2000 deg/s, and a 3-axis magnetometer. Infra-Red (IR) markers are attached with QDrone, and the cable-suspended load to get tracked by the camera system, as shown in Figure 11.

The data stream coming from all 16 cameras is fed into the software, Motive, that comes with the camera system. The motive software runs an optimization algorithm and calculates an accurate pose of the system, which consists of a quadrotor and a cable suspended load. The pose information provided by the motive software consists of the three-dimensional position

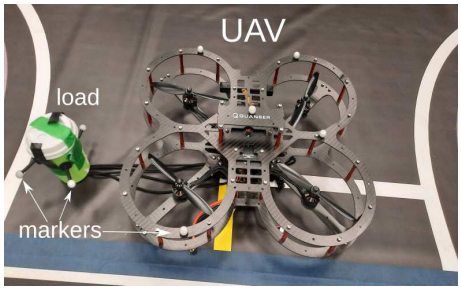

Fig. 11. Quanser QDrone with cable suspended load and IR markers.

TABLE II
PARAMETERS OF QDRONE AND CABLE SUSPENDED LOAD

Description	Physical value
cable length L	0.4 m
mass of the quadrotor m_q	0.85 kg
mass of the payload m_ℓ	0.13 kg
inertia of the quadrotor $J = \text{diag}(J_x, J_y, J_z)$	(0.01,0.0082,0.0148) kg.m^2
maximum payload capacity	0.3 kg

of the quadrotor and load and the orientation of the quadrotor. This information is sent to the onboard controller mounted on the quadrotor via a high-speed WiFi link. Opti-track data and the IMU-sensor data are fused together using vendor-provided complementary filter modules. Moreover, using Hall-effect sensors, motor speed and thrust is measured. In summary, at this point, the system makes all the required state information available at 100 Hz.

B. Hardware Implementation

Before presenting the experimental results, we provide relevant system parameters in Table II. In this experiment, the assigned path to be followed by the load is a unit circle at the height of 0.3 meters with a center coinciding with the center of the arena. At the outset of the experiment, both the quadrotor and the cable are lying on the ground. The tension in the cable at this stage is zero. Therefore, the quadrotor initializes in a mode that takes it off to a height such that it hovers with load hanging above the ground. In this way, before the controller is invoked, it is ensured the tension in the string is non-zero (Assumption 1), and the swing in the load is sufficiently damped. The position of the load and the quadrotor is shown in Figure 12 throughout the duration of the flight using blue and red colored curves, respectively. The initial position of the two rigid bodies, i.e., the load and the quadrotor, on the ground are indicated by markers in the figure. Once the quadrotor starts hovering and the load swing is reasonably reduced, the proposed controller is invoked, and the load starts approaching and traversing along the assigned circular path. The gains of the controller are carefully designed using classical pole-placement techniques and further refined by tuning. These gains are shown in Table III. At the termination of the mission, both the load and the quadrotor land on the ground.

Due to the sensor noise and small errors involved in state estimation, an error could be introduced in the position of the load with reference to the assigned path. For the experiment

TABLE III
CONTROLLER GAINS

Description	Symbols	Values
ξ-system gains (39)	$\left\{k_1^\xi, k_2^\xi, k_3^\xi,\right.$	$\{41.0473, 133.8854, 181.2496,$
	$\left.k_4^\xi, k_5^\xi, k_6^\xi\right\}$	$130.3594, 52.5375, 11.2500\}$
ζ-system gains (40)	$\left\{k_1^\zeta, k_2^\zeta, k_3^\zeta,\right.$	$\{41.0473, 133.8854, 181.2496,$
	$\left.k_4^\zeta, k_5^\zeta, k_6^\zeta\right\}$	$130.3594, 52.5375, 11.2500\}$
η-system gains (41)	$\{k_1^\eta, k_2^\eta, k_3^\eta,$	$\{0.0, 43.8716, 74.2399$
	$k_4^\eta, k_5^\eta, k_6^\eta\}$	$66.7440, 33.6240, 9.0000\}$
μ-system gains (42)	$\{k_1^\mu, k_2^\mu\}$	$\{0.2750, 1.0500\}$

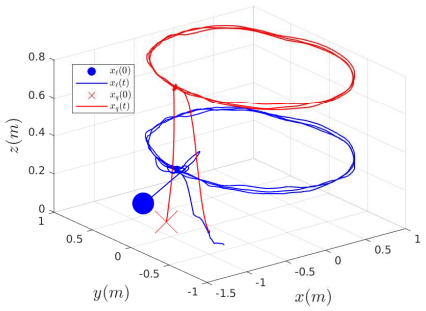

Fig. 12. Position of the suspended load and the Quanser QDrone in a three-dimensional arena. The initial position of the load and the quadrotor are indicated by markers. The circular path followed by the load is also shown.

under discussion, the position error in the x-y plane is plotted in Figure 13, and the error in the height of the load is shown in Figure 14. As shown in Figure 13 and Figure 14, the initial error is large as the QDrone prepares for the mission. The error starts reducing as the controller is invoked about 20 seconds after the start of the experiment. In the steady-state, the system performs very well as the magnitudes of the position errors are small even in the presence of latency and noise, as shown in Figure 13 and Figure 14.

Finally, we show the control effort, i.e., total thrust u_t and body torques τ, generated by QDrone in Figure 15 and Figure 16, respectively. It can be seen that the control effort generated by the system corresponds to the overall inertia of the drone and the mass of the suspended load. Also, the control effort indicates that the controller can successfully stabilize the path following manifold without exceeding the actuation limits of the QDrone system, i.e., 16 N thrust limit and 0.8 N-m body torques limit. Note that in all experimental results reported in this section, the presented figures contain valid data once the controller is invoked (around 20 sec). The overall system works in the hover mode (i.e., the tension in the cable is non-zero). As seen in Figure 16, the control torque τ_3 is relatively smaller compared to τ_1 and τ_2 because the quadrotor pose is commanded to a constant value. In contrast, the quadrotor needs to produce small movements in the roll and pitch axis to follow the given circular path.

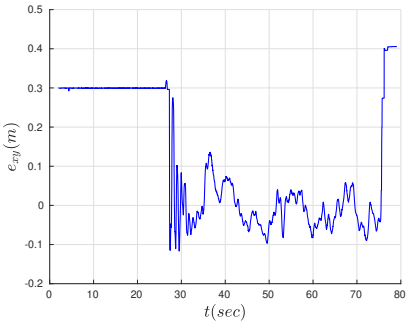

Fig. 13. Path following error in xy-direction is shown in the figure. This error indicates the difference between the assigned path and the actual position of the load in the x-y plane. The initial error is large when the QDrone is hovering above the ground, and the error reduces in magnitude as the controller takes over. The sign of the error indicates whether the load is inside or outside the assigned path.

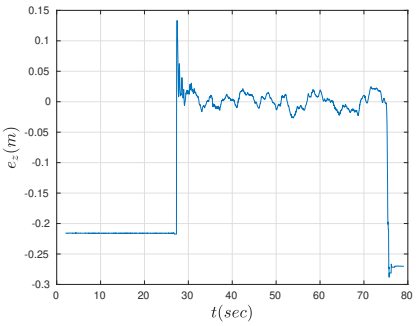

Fig. 14. Path following error in the z direction is shown in the figure. The error indicates the difference in the assigned path and the height of the load. The controller reduces the initial error in height, and the load approaches the path and follows it.

IX. CONCLUSION

This paper addresses the path following problem for a quadrotor suspended to a point mass through a taut cable using a global parameterization of the underlying manifold. We introduced two distinct families of smooth functions that guarantee a well-defined vector relative degree, as well as coordinate and feedback transformation, for the system under study. We demonstrate that there exist functions belonging to the family $\mathscr{F}_R$ that induce controllers with a local region of convergence, while $\mathscr{F}_r$ contains functions that, in terms of region of convergence, yield almost-global controllers. These families induce smooth dynamic feedback controllers that solve the load path following problem for a large class of both closed and non-closed curves. In particular, the proposed controllers offer three distinct features: i) the load converges to the desired path and achieves path invariance, ii) motion of the load along the path, which involves point stabilization on the path, following a desired velocity or acceleration profile along the path, and iii) maintaining a desired orientation of the quadrotor or its rate throughout the mission. Simulation results demonstrate the performance of the proposed controllers in the presence of noise and modeling uncertainties. Finally, we bridge the gap between theoretical results of this paper and real world hardware experiment, by demonstrating the practical

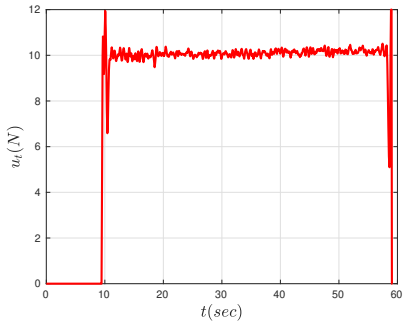

Fig. 15. Thrust control input u_t generated by the QDrone while following a circular path with a cable suspended load.

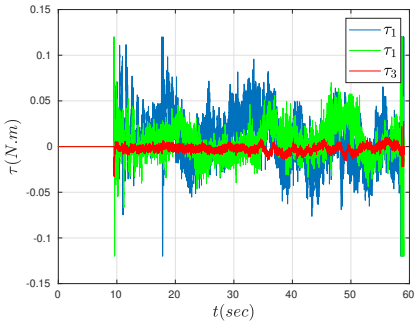

Fig. 16. Control torques τ_1, τ_2, τ_3 generated by the QDrone UAV to make the cable suspended load follow the given circular path. It can be seen that the control efforts are well within the saturation bounds.

performance of the proposed controller on a Quanser QDrone system.

ACKNOWLEDGMENT

The authors would like to thanks Samira Eshghi for helping out in the experiments.

X. APPENDIX

A. Proof of Proposition IV.1

Proof. Consider system (3) and let

$$\bar{f}(x) := \operatorname{col}\left(v_\ell, -\frac{T}{m_\ell L}(x_\ell - x_q) - gb_3, v_q, -gb_3 + \frac{T}{m_q L}(x_\ell - x_q), \Diamond|_{\mathsf{SO(3)}}(R\widehat{\Omega}), J^{-1} - (\Omega \times J\Omega)\right),$$

$\bar{g}_1(x) := \operatorname{col}\left(0_{21}, \frac{1}{J_x}, 0, 0\right)$, $\bar{g}_2(x) := \operatorname{col}\left(0_{22}, \frac{1}{J_y}, 0\right)$, $\bar{g}_3(x) := \operatorname{col}\left(0_{23}, \frac{1}{J_z}\right)$, and $\bar{g}_4(x) := \operatorname{col}\left(0_9, \frac{1}{m_q} R b_3, 0_{12}\right)$, be smooth vector fields on $\bar{\mathsf{Q}}$. Then, we can express the quadrotor system (3) attached with a cable-suspended payload in the control-affine form as

$$\dot{x} = \bar{f}(x) + \bar{g}_1(x)\tau_1 + \bar{g}_2(x)\tau_2 + \bar{g}_3(x)\tau_3 + \bar{g}_4(x)u_t.$$

By taking iterative Lie derivative of the functions $\bar{\alpha}_i$, for $i \in \{1,2,3\}$, we get

$$L_{\bar{g}_j} L_{\bar{f}}^k \bar{\alpha}_i = 0, \tag{51}$$

for $k \in \{0,1,2\}$ and $j \in \{1,2,3,4\}$. Similarly, (51) holds true for $j \in \{1,2,3\}$ and $k = 3$. The first nonzero Lie derivative appears when we take the fourth derivative along the vector field $\bar{g}_4(x)$, i.e., $L_{\bar{g}_4} L_{\bar{f}}^3 \bar{\alpha}_i \neq 0$, for $i \in \{1,2,3\}$. For the function $\bar{\alpha}_4$, the first non-zero Lie derivative appears when we take the second derivative along the vector fields $\bar{g}_2(x)$ and $\bar{g}_3(x)$, while the Lie derivatives along the vector fields $\bar{g}_1(x)$ and $\bar{g}_4(x)$ are identically zero. Therefore, the decoupling matrix takes the following form:

$$\bar{D}(x) = \begin{bmatrix} 0 & 0 & 0 & L_{\bar{g}_4} L_{\bar{f}}^3 \bar{\alpha}_1 \\ 0 & 0 & 0 & L_{\bar{g}_4} L_{\bar{f}}^3 \bar{\alpha}_2 \\ 0 & 0 & 0 & L_{\bar{g}_4} L_{\bar{f}}^3 \bar{\alpha}_3 \\ 0 & L_{\bar{g}_2} L_{\bar{f}} \bar{\alpha}_4 & L_{\bar{g}_3} L_{\bar{f}} \bar{\alpha}_4 & 0 \end{bmatrix}. \tag{52}$$

It is easy to see that $\bar{D}(x)$ is singular for all x in $\bar{\mathsf{Q}}$ and the system (3) lacks a well-defined vector relative degree. □

B. Proof of Proposition V.5

Proof. From Proposition V.4, it is evident that when the inputs are bounded, the body rates p, q, r are also bounded. To establish that $\dot{\delta}_1$ is bounded, we use the first equation in (30)

$$|\dot{\delta}_1| \leq |r||r_{12}| + |q||r_{13}|. \tag{53}$$

Since rotation matrices are orthonormal, each $|r_{ij}| \leq 1$, therefore, $\dot{\delta}_1$ is bounded. For the same reason, we can show that $\delta_1 \leq |r_{11}| \leq 1$ is also bounded. The same arguments applies to the internal states, i.e., $\dot{\delta}_i$ and δ_i for $i \in \{2, \ldots, 5\}$ are also bounded. The sixth internal state $\delta_6 = z_1$ is also bounded because z_1 is the cumulative force generated by all four rotors of the quadrotor, which is a bounded quantity. It follows that $\dot{\delta}_6 = z_2 = \dot{z}_1$ is also bounded since the inputs are assumed to be continuously differentiable. □

REFERENCES

[1] D. Mellinger and V. Kumar, "Minimum snap trajectory generation and control for quadrotors," in *2011 IEEE International Conference on Robotics and Automation*, May 2011, pp. 2520–2525. 1, 2

[2] H. J. Mendes and O. Egbue, "Analysis of inverted rotors in multirotor aerial vehicles with VTOL," *IEEE Transactions on Vehicular Technology*, vol. 67, no. 6, pp. 5535–5539, June 2018. 1

[3] K. Tanaka, M. Tanaka, Y. Takahashi, A. Iwase, and H. O. Wang, "3-D flight path tracking control for unmanned aerial vehicles under wind environments," *IEEE Transactions on Vehicular Technology*, vol. 68, no. 12, pp. 11 621–11 634, Dec 2019. 1

[4] D. K. D. Villa, A. S. Brandão, and M. Sarcinelli-Filh, "A survey on load transportation using multirotor UAVs," *Journal of Intelligent and Robotic Systems: Theory and Applications*, vol. 98, no. 30, pp. 267–296, 2020. 1

[5] W. Shi, J. Li, N. Cheng, F. Lyu, S. Zhang, H. Zhou, and X. Shen, "Multi-drone 3-D trajectory planning and scheduling in drone-assisted radio access networks," *IEEE Transactions on Vehicular Technology*, vol. 68, no. 8, pp. 8145–8158, Aug 2019. 1

[6] Z. Lv, Y. Wu, R. Wang, and Y. Li, "Nonlinear motion control for a quadrotor transporting a cable-suspended payload," *IEEE Transactions on Vehicular Technology*, pp. 1–1, 2020. 1

[7] T. Lee, "Geometric control of quadrotor UAVs transporting a cable-suspended rigid body," *IEEE Transactions on Control Systems Technology*, vol. 26, no. 1, pp. 255–264, Jan 2018. 1

[8] T. Chen and J. Shan, "A novel cable-suspended quadrotor transportation system: From theory to experiment," *Aerospace Science and Technology*, vol. 104, p. 105974, 2020. 1

[9] S. Yang and B. Xian, "Exponential regulation control of a quadrotor unmanned aerial vehicle with a suspended payload," *IEEE Transactions on Control Systems Technology*, pp. 1–8, 2019. 1

[10] K. Sreenath, N. Michael, and V. Kumar, "Trajectory generation and control of a quadrotor with a cable-suspended load - a differentially-flat hybrid system," in *2013 IEEE International Conference on Robotics and Automation*, 2013, pp. 4888–4895. 1, 2

[11] M. Guo, D. Gu, W. Zha, X. Zhu, and Y. Su, "Controlling a quadrotor carrying a cable-suspended load to pass through a window," *Journal of Intelligent & Robotic Systems*, 05 2019. 1

[12] Y. Li and C. Nielsen, "Synchronized closed path following for a differential drive and manipulator robot," *IEEE Transactions on Control Systems Technology*, vol. 25, no. 2, pp. 704–711, March 2017. 1

[13] B. Xian, S. Wang, and S. Yang, "An online trajectory planning approach for a quadrotor uav with a slung payload," *IEEE Transactions on Industrial Electronics*, vol. 67, no. 8, pp. 6669–6678, 2020. 1

[14] J. J. Corona-Sánchez, R. Kristiansen, and T. S. Andersen, "Path planning and reactive based control for a quadrotor with a suspended load," in *2021 International Conference on Unmanned Aircraft Systems (ICUAS)*, 2021, pp. 507–516. 1

[15] A. Akhtar and C. Nielsen, "Path following for a car-like robot using transverse feedback linearization and tangential dynamic extension," in *50th IEEE Conference on Decision and Control and European Control Conference, (CDC)-ECC*, Dec. 2011, pp. 7949 –7979. 2

[16] A. P. Aguiar, J. P. Hespanha, and P. V. Kokotović, "Performance limitations in reference tracking and path following for nonlinear systems," *Automatica*, vol. 44, no. 3, pp. 598–610, 2008. 2

[17] C. Nielsen, C. Fulford, and M. Maggiore, "Brief paper: Path following using transverse feedback linearization: Application to a maglev positioning system," *Automatica*, vol. 46, no. 3, pp. 585–590, 2010. 2

[18] A. Hladio, C. Nielsen, and D. Wang, "Path following for a class of mechanical systems," *IEEE Transactions on Control Systems Technology*, vol. 21, no. 6, pp. 2380–2390, 2013. 2

[19] A. Akhtar, C. Nielsen, and S. L. Waslander, "Path following using dynamic transverse feedback linearization for car-like robots," *IEEE Transactions on Robotics*, vol. 31, no. 2, pp. 269–279, April 2015. 2, 5

[20] A. Akhtar, S. Saleem, and S. L. Waslander, "Path following for a class of underactuated systems using global parameterization," *IEEE Access*, vol. 8, pp. 34 737–34 749, 2020. 2, 4, 6, 8

[21] D. C. Gandolfo, L. R. Salinas, A. Brandão, and J. M. Toibero, "Stable path-following control for a quadrotor helicopter considering energy consumption," *IEEE Transactions on Control Systems Technology*, vol. 25, no. 4, pp. 1423–1430, July 2017. 2

[22] F. Bullo and A. D. Lewis, *Geometric Control of Mechanical Systems*, ser. Texts in Applied Mathematics. New York-Heidelberg-Berlin: Springer Verlag, 2004, vol. 49. 2, 6

[23] A. Akhtar and S. L. Waslander, "Controller class for rigid body tracking on $\mathsf{SO}(3)$," *IEEE Transactions on Automatic Control*, vol. 66, no. 5, pp. 2234–2241, 2021. 2

[24] S. P. Bhat and D. S. Bernstein, "A topological obstruction to continuous global stabilization of rotational motion and the unwinding phenomenon," *Systems and Control Letters*, vol. 39, no. 1, pp. 63 – 70, 2000. 2

[25] K. Sreenath, T. Lee, and V. Kumar, "Geometric control and differential flatness of a quadrotor uav with a cable-suspended load," in *52nd IEEE Conference on Decision and Control*, Dec 2013, pp. 2269–2274. 2, 5

[26] N. A. Chaturvedi, A. K. Sanyal, and N. H. McClamroch, "Rigid-body attitude control," *IEEE Control Systems*, vol. 31, no. 3, pp. 30–51, June 2011. 2

[27] P. Casau, R. Cunha, R. G. Sanfelice, and C. Silvestre, "Hybrid control for robust and global tracking on smooth manifolds," *IEEE Transactions on Automatic Control*, vol. 65, no. 5, pp. 1870–1885, 2020. 2

[28] F. Bullo, R. Murray, and A. Sarti, "Control on the sphere and reduced attitude stabilization," *IFAC Proceedings Volumes*, vol. 2, 10 2001. 2

[29] T. Lee, K. Sreenath, and V. Kumar, "Geometric control of cooperating multiple quadrotor uavs with a suspended payload," in *52nd IEEE Conference on Decision and Control*, Dec 2013, pp. 5510–5515. 2

[30] J. Zeng and K. Sreenath, "Geometric control of a quadrotor with a load suspended from an offset," in *2019 American Control Conference (ACC)*, July 2019, pp. 3044–3050. 2

[31] J. Zeng, P. Kotaru, and K. Sreenath, "Geometric control and differential flatness of a quadrotor uav with load suspended from a pulley," in *2019 American Control Conference (ACC)*, July 2019, pp. 2420–2427. 2

[32] S. Tang and V. Kumar, "Mixed integer quadratic program trajectory generation for a quadrotor with a cable-suspended payload," in *2015 IEEE International Conference on Robotics and Automation (ICRA)*, 2015, pp. 2216–2222. 2

[33] B. Xian and S. Yang, "Robust tracking control of a quadrotor unmanned aerial vehicle-suspended payload system," *IEEE/ASME Transactions on Mechatronics*, pp. 1–1, 2020. 2

[34] X. Liang, Y. Fang, N. Sun, and H. Lin, "Nonlinear hierarchical control for unmanned quadrotor transportation systems," *IEEE Transactions on Industrial Electronics*, vol. 65, no. 4, pp. 3395–3405, 2018. 2

[35] L. Qian and H. H. Liu, "Path-following control of a quadrotor uav with a cable-suspended payload under wind disturbances," *IEEE Transactions on Industrial Electronics*, vol. 67, no. 3, pp. 2021–2029, 2020. 2

[36] K. Sreenath, N. Michael, and V. Kumar, "Trajectory generation and control of a quadrotor with a cable-suspended load - a differentially-flat hybrid system," in *2013 IEEE International Conference on Robotics and Automation*, May 2013, pp. 4888–4895. 4

[37] A. Akhtar, S. L. Waslander, and C. Nielsen, "Path following for a quadrotor using dynamic extension and transverse feedback linearization," in *51st IEEE Conference on Decision and Control (CDC)*, Dec. 2012, pp. 3551 –3556. 4, 5, 8

[38] J. Stuelpnagel, "On the parametrization of the three-dimensional rotation group," *SIAM Review*, vol. 6, no. 4, pp. 422–430, 1964. 4

[39] C. Nielsen, C. Fulford, and M. Maggiore, "Path following using transverse feedback linearization: Application to a maglev positioning system," *Automatica*, vol. 46, no. 3, pp. 585–590, March 2010. 6

[40] G. Strang, *Linear Algebra and its applications*. 111 Fifth Avenue, New York, New York 10003: Academic Press, INC, 1976. 6

[41] A. Akhtar, S. Waslander, and C. Nielsen, "Fault tolerant path following for a quadrotor," in *52nd IEEE Conference on Decision and Control (CDC)*, Dec 2013, pp. 847–852. 8

[42] Akhtar, Adeel, "Nonlinear and geometric controllers for rigid body vehicles," Ph.D. dissertation, University of Waterloo, 2018. 12

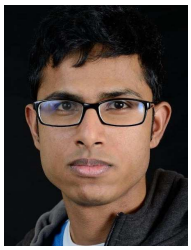

Adeel Akhtar (S'12 - M'18) his M.A.Sc. degree in ECE Department, from Univ. of Waterloo, Canada, in 2012. He received his Ph.D from Mechanical and Mechatronics Engineering Department, Univ. of Waterloo, Canada, in 2018.

Currently, he is a post-doctoral research scientist with ECE Department, at Univ. of California at Santa Cruz. Prior to that he held postdoctoral positions at the Univ. of Toronto, Canada, and York Univ., Canada.

Sajid Saleem (S'09 - M'14 - SM '20) received the M.S. degree in mathematics and the Ph.D. degree in ECE from the Georgia Institute of Technology, Atlanta, GA USA, in 2011 and 2013, respectively.

He is currently an Assistant Professor with the College of Computer Science and Engineering, University of Jeddah, Jeddah, Saudi Arabia.

His research interests include systems analysis, signal processing, and differential geometry.

Jinjun Shan (Senior Member, IEEE) received Ph.D. degree in spacecraft design from Harbin Institute of Technology, Harbin, China, in 2002.

He is currently a professor of Space Engineering and Chair of Dept. of Earth and Space Science and Engineering, York Univ., Toronto, Canada.

Dr. Shan was the recipient of Alexander von Humboldt Fellowship. and Japan Society for the Promotion of Science Fellowship in 2012.